OPEN ACCESS



Distinct Acceleration Relations of Galaxies and Galaxy Clusters from Hyperconical Modified Gravity

Robert Monjo^{1,2,3} and Indranil Banik^{4,5}

Area of Physics, University of Alfonso X El Sabio, C/ Arapiles 13, Chamberí, 28015 Madrid
 Department of Mathematics, Saint Louis University—Madrid Campus, Max Aub street, 5, E-28003, Madrid, Spain
 Department of Physics and Mathematics, University of Alcalá, Faculty of Sciences, E-28805 Alcalá de Henares, Madrid, Spain
 Scottish Universities Physics Alliance, University of Saint Andrews, North Haugh, Saint Andrews, Fife, KY16 9SS, UK
 Institute of Cosmology & Gravitation, University of Portsmouth, Dennis Sciama Building, Burnaby Road, Portsmouth PO1 3FX, UK
 Received 2025 May 15; revised 2025 July 28; accepted 2025 August 7; published 2025 October 3

Abstract

General relativity (GR) is the most successful theory of gravity, with great observational support on local scales. However, to keep GR valid over cosmic scales, some phenomena require the assumption of exotic dark matter, especially the cosmic expansion history and flat rotation curves of galaxies. Their radial acceleration relation (RAR) indicates a tight correlation between the dynamical mass and the baryonic mass. This suggests that galactic observations could be better explained by modified gravity theories without exotic matter. Modified Newtonian dynamics (MOND) is an alternative theory that was originally designed to do exactly this using a new fundamental acceleration scale, a_0 , the so-called Milgromian parameter. However, this nonrelativistic model lacks the flexibility needed to account for the wide variety of observed phenomena. In contrast, a relativistic MOND-like gravity naturally emerges from the hyperconical model, which derives a fictitious acceleration compatible with observations. We analyze the compatibility of the hyperconical model with respect to distinct RAR observations of 10 galaxy clusters obtained from HIFLUGCS and 60 high-quality SPARC galaxy rotation curves. The results show that a general relation can be fitted to most cases with only one or two parameters, with an acceptable χ^2 and p-value. These findings suggest a possible way to complete the proposed modification of GR on cosmic scales.

Unified Astronomy Thesaurus concepts: Modified Newtonian dynamics (1069); Galaxy dynamics (591); Galaxy clusters (584)

1. Introduction

1.1. The Missing Gravity Problem

As is well known, observational tests of general relativity (GR) show successful results on solar system scales (H. Dittus & C. Lämmerzahl 2007; I. Ciufolini et al. 2019; X.-H. Liu et al. 2022; P. Touboul et al. 2022; H. Desmond et al. 2024; D. Vokrouhlický et al. 2024). The success of standard gravity seems to be in question only on larger scales (K.-H. Chae et al. 2020; I. Banik & H. Zhao 2022). It is well known that exotic cold dark matter (CDM) is required to extend GR to cosmic scales. However, hypothetical CDM particles present strong challenges, in particular the tight empirical relationship between observed gravitational anomalies and the distribution of visible baryonic matter in galaxies (S. Trippe 2014; D. Merritt 2017; J. S. Goddy et al. 2023). This empirical law is known as the mass-discrepancy acceleration relation (MDAR; S. S. McGaugh 2004; A. Di Cintio & F. Lelli 2015; H. Desmond 2016), the mass-luminosity relation (A. Leauthaud et al. 2010; A. Cattaneo et al. 2014), the baryonic Tully–Fisher relation (BTFR; F. Lelli et al. 2019; J. S. Goddy et al. 2023), or the more general radial acceleration relation (RAR; S. S. McGaugh et al. 2016; F. Lelli et al. 2017; Y. Tian et al. 2020).

Original content from this work may be used under the terms of the Creative Commons Attribution 4.0 licence. Any further distribution of this work must maintain attribution to the author(s) and the title of the work, journal citation and DOI.

Y. Tian et al. (2020) found that the observed RAR in galaxy clusters is consistent with predictions from a semianalytical model developed in the framework of standard Lambda CDM (ΛCDM; G. Efstathiou et al. 1990; J. P. Ostriker & P. J. Steinhardt 1995). To explain how the contribution of CDM is determined by that of baryons, some authors suggest that they present a strong coupling that leads to an effective law like the MDAR/BTFR/RAR (L. Blanchet 2007; A. Katz et al. 2016; R. Barkana 2018; B. Famaey et al. 2020). It has also been argued that such a correlation can arise in the ΛCDM framework once baryonic feedback effects are simulated with adequate resolution (F. J. Mercado et al. 2024).

The absence of any direct or indirect nongravitational detection of dark matter suggests that it may have a very weak or even nonexistent interaction with baryons (C. Abel et al. 2017; S. Hoof et al. 2020; P. Du et al. 2022; J. Aalbers et al. 2023; X.-S. Hu et al. 2024), which is in conflict with these tight empirical relationships. Moreover, excess rotation occurs only where the Newtonian acceleration a_N induced by the visible matter satisfies $a_{\rm N} \lesssim a_0 \approx 1.2 \times 10^{-10} \, {\rm m \, s^{-2}}$, suggesting that the missing gravity problem is a spacetime problem rather than a matter-type problem. This is also consistent with the deficient dark matter halos observed in some relic galaxies, even though their accelerations exceed the a_0 threshold (S. Comerón et al. 2023). In other cases, the CDM halo hypothesis predicts a systematically deviating relation from the observations, with densities about half of what is predicted by CDM simulations (W. J. G. de Blok et al. 2008). In general, galaxy rotation curves and velocity dispersions appear to be more naturally explained by modified gravity

(S. S. McGaugh et al. 2007, 2016; B. Famaey & S. S. McGaugh 2012; I. Banik & H. Zhao 2022; K.-H. Chae 2022).

The dark matter hypothesis also presents difficulties in explaining some phenomena such as the absence of the expected Chandrasekhar dynamical friction in cluster collisions, falsified by more than 7σ (P. Kroupa 2015; E. Ardi & H. Baumgardt 2020; P. Kroupa et al. 2023). The lack of dynamical friction on galaxy bars strongly suggests that the central density of CDM in typical disk galaxies is much lower than expected in standard CDM simulations (M. Roshan et al. 2021). Another example is the morphology of dwarf galaxies. According to E. Asencio et al. (2022), the observed deformations of dwarf galaxies in the Fornax Cluster and the lack of low surface brightness dwarfs near its center are incompatible with Λ CDM predictions. Moreover, the dwarfs analyzed in that study have sufficiently little stellar mass that the observations cannot be explained by baryonic feedback effects, but they are consistent with Milgromian or modified Newtonian dynamics (MOND; M. Milgrom 1983). Therefore, most observations suggest the need to explore modified gravity as an alternative to the standard model (S. Trippe 2014; D. Merritt 2017).

1.2. Beyond the MOND Paradigm

The MOND paradigm has been deeply explored from galactic dynamics to the Hubble tension, which is explained by a more efficient (early) formation of large structures such as the local supervoid (R. C. Keenan et al. 2013; M. Haslbauer et al. 2020; I. Banik & H. Zhao 2022; S. Mazurenko et al. 2024, 2025; I. Banik & V. Kalaitzidis 2025). The RAR has been thoroughly analyzed using galaxy rotation curves collected from the Spitzer Photometry and Accurate Rotation Curves (SPARC) sample (F. Lelli et al. 2016, 2019). The results were anticipated over three decades ago by MOND (M. Milgrom 1983; S. S. McGaugh et al. 2016), although the form of the transition between the Newtonian and Milgromian regimes must be found empirically.

However, the relativistic formulation of MOND has been less successful. In particular, Bekenstein proposed a non-cosmological version of tensor–vector–scalar (TeVeS) gravity (J. D. Bekenstein 2004; B. Famaey & S. S. McGaugh 2012) that predicts unstable stars on a timescale of a few weeks (M. D. Seifert 2007), which is only avoidable with an undetermined number of terms (N. E. Mavromatos et al. 2009). To solve these issues, C. Skordis & T. Złośnik (2021) found that, by adding terms analogous to the Friedmann–Lemaître–Robertson–Walker (FLRW) action, at least the second-order expansion is free of ghost instabilities. Their model is also capable of obtaining gravitational waves traveling at the speed of light c, which was not the case with the original TeVeS. However, the authors pointed out that it needs to be embedded in a more fundamental theory.

Recently, L. Blanchet & C. Skordis (2024) proposed a relativistic MOND formulation based on spacetime foliation by three-dimensional space-like hypersurfaces labeled by the Khronon scalar field. The idea is very similar to the Arnowitt–Deser–Misner treatment in the dynamical embedding of the hyperconical Universe (R. Monjo 2017, 2018, 2023, 2024a, 2024b; R. Monjo & R. Campoamor-Stursberg 2020).

Applying perturbation theory to the hyperconical metric gives a relativistic theory with MOND phenomenology, which adequately fits 123 SPARC galaxy rotation curves

(R. Monjo 2023). The cosmic acceleration derived from it is $a_{\gamma 0} \equiv 2\gamma_0^{-1}c/t$, where t is the age of the Universe and $\gamma_0 > 1$ is a projection parameter that translates from the ambient spacetime to the embedded manifold (R. Monjo & R. Campoamor-Stursberg 2023; R. Monjo 2024b). In contrast to the Milgrom constant a_0 , the cosmic acceleration $a_{\gamma 0}$ is a variable that depends on the geometry considered, especially the ratio between the Kepler–Newton orbital speed and the Hubble flux. Numerical equivalence between the a_0 and $a_{\gamma 0}$ scales is found for $\gamma_0 \approx 13 \pm 3$ or, equivalently, for $\gamma_0^{-1} \approx 0.08 \pm 0.02$. In the limit of weak gravitational fields and low velocities,

the hyperconical model is also linked to the scalar tensor vector gravity (STVG) theory, popularly known as Moffat gravity (MOG; J. W. Moffat 2006). The MOG/STVG model is a fully covariant or Lorentz-invariant theory that includes a dynamical massive vector field and scalar fields to modify GR with a dynamical "gravitational constant" G (J. W. Moffat & V. T. Toth 2009, 2013; S. Harikumar & M. Biesiada 2022). In particular, MOG leads to an anomalous acceleration of about $2 G \alpha_G D^2 \approx 1.1 \times 10^{-10} \,\mathrm{m \ s^{-2}} \approx 2 \gamma_0^{-1} c/t$ for $\gamma_0 \approx 12$, with $\alpha_G \approx 10$ and the universal MOG constant $D = 6.25 \times 10^3 M_\odot^{1/2} \,\mathrm{kpc^{-1}}$. Fixing these parameters using galaxy rotation curves, MOG fails to account for the observed velocity dispersion profile of Dragonfly 44 at 5.5σ confidence, even if one allows plausible variations to its star formation history and thus stellar mass-to-light ratio (H. Haghi et al. 2019). MOG also struggles to explain the Galactic rotation curve, where the discrepancy is smaller but the measurements are more accurate (C. Negrelli et al. 2018).

The number of parameters needed to accommodate most theories to observations of galaxy clusters is perhaps too large and unnatural. In all cases, additional theoretical motivation is necessary for the phenomenological parameters, e.g., the CDM distribution profile, the ad hoc MOND interpolating function μ , and the MOG constant D. In contrast, the hyperconical model proposed by Monjo derives a natural modification to GR from minimal dynamical embedding in a (flat) fivedimensional Minkowskian spacetime (R. Monjo 2023, 2024a, 2024b). The hyperconical model is a kind of coasting Universe like Melia's $R_h = ct$ model (F. Melia 2007; F. Melia & M. López-Corredoira 2022). An important difference is that those models assume GR to be valid cosmologically (F. Melia 2017), while the hyperconical model assumes GR to be valid only at a local scale (R. Monjo 2024b). Since the late Universe expansion history is very close to linear even in ΛCDM (R. Monjo 2017; Planck Collaboration et al. 2020) and according to myriad observations, it is reasonable to explore how linear expansion impacts the local GR.

Therefore, this paper aims to show how the anomalous RAR in 10 galaxy clusters analyzed by D. Eckert et al. (2022) and P. Li et al. (2023) can be adequately modeled by local GR in hyperconical modified gravity (HMG; R. Monjo 2023). As Y. Tian et al. (2020) pointed out, clusters present a larger anomalous acceleration ($g \sim 10^{-9} \, \mathrm{m \, s^{-2}}$) than galaxy rotation curves ($g \sim 10^{-10} \, \mathrm{m \, s^{-2}}$), reflecting the missing baryon problem that remains a challenge for MOND in galaxy clusters (B. Famaey & S. S. McGaugh 2012; P. Li et al. 2023; R. Kelleher & F. Lelli 2024; Y. Tian et al. 2024). This open issue is addressed here with the following structure. Section 2 summarizes the data used and the HMG model, Section 3 shows the main results in the fits and discusses predictions for

galaxies and smaller systems, and finally, Section 4 points out the most important findings and gives our concluding remarks.

2. Data and Model

2.1. Observations Used

We used observational estimates of the RAR (total gravity observed compared to Newtonian gravity due to baryons) for 10 galaxy clusters that were collected from the HIghest X-ray FLUx Galaxy Cluster Sample (HIFLUGCS; P. Li et al. 2023). In particular, the galaxy clusters considered are as follows: A0085, A1795, A2029, A2142, A3158, A0262, A2589, A3571, A0576, and A0496. These clusters have redshift *z* in the range 0.0328–0.0899. We also compare our results to rotation curves collected from 60 high-quality SPARC galaxies filtered to well-measured intermediate radii (S. S. McGaugh et al. 2007, 2016; F. Lelli et al. 2019).

2.2. RAR from HMG

Our main aim is to assess whether the empirical RAR agrees with the HMG as developed by R. Monjo (2023) and summarized here. Let g be the background metric of the so-called hyperconical Universe (R. Monjo 2017, 2018; R. Monjo & R. Campoamor-Stursberg 2020, 2023). Working in units where c = 1 and the age of the Universe is $t_0 = 1$, the metric g is locally approximately given by

$$g \approx dt^{2}(1 - kr'^{2}) - \frac{t^{2}}{t_{0}^{2}} \left(\frac{dr'^{2}}{1 - kr'^{2}} + r'^{2}d\Sigma^{2} \right) - \frac{2r'tdr'dt}{t_{0}^{2}\sqrt{1 - kr'^{2}}}, \quad (1)$$

where $k = 1/t_0^2$ is the spatial curvature for the current age t of the Universe, t/t_0 is the scale factor associated with lengths because the expansion history is linear (R. Monjo 2024b), $r' \ll t_0$ is the comoving distance, and Σ represents the angular coordinates. It is important to note that this background metric is naturally induced from dynamical embedding of a linearly expanding three-sphere into a five-dimensional Minkowskian spacetime when comoving observers measure distances (R. Monjo 2024a, 2024b). Thus, our metric deviates from the standard FLRW construction, which assumes a static embedding of spatially maximally symmetric three-manifolds (obtaining $dr'^2/(1-kr'^2)+r'^2d\Sigma^2$) and a dynamical factor a(t) that is included ad hoc to represent the expansion. In our framework, comoving observers lead to shift and lapse terms in Equation (1), representing an apparent radial spatial inhomogeneity that appears as a fictitious acceleration with adequate stereographic projection coordinates (R. Monjo & R. Campoamor-Stursberg 2023).

Moreover, since the Universe is not empty, such a projection depends on the matter source. In particular, any gravitational system of mass $M_{\rm sys}$ (enclosed at a given radius) generates a perturbation over the background metric (Equation (1)) that can be written as $g \to \hat{g}$ such that $kr'^2 \to \hat{k}\hat{r}'^2 \equiv k\hat{r}'^2 + 2GM_{\rm sys}(\hat{r}')/\hat{r}'$. Applying the validity of GR at a local scale (Appendix A), the perturbation term $\hat{h} \equiv \hat{g} - g$ is a key aspect of the HMG model (Appendix B).

Also important is the stereographic projection of the coordinates $r' \to \hat{r}' = \lambda^{1/2} r'$ and $t \to \hat{t} = \lambda t$, both of which are given by a scaling factor $\lambda \equiv 1/(1 - \gamma/\gamma_0)$ that is a function

of the angular position $\gamma=\sin^{-1}(r'/t_0)$ and a projection factor $\gamma_0^{-1}=\gamma_{\rm sys}^{-1}\cos\gamma_{\rm sys}$, where $\gamma_{\rm sys}$ is the characteristic angle of the gravitational system (Appendix C). In an empty Universe, $\gamma_0=\gamma_U/\cos\gamma_U$. We expect $\gamma_U=\pi/3$ and therefore $\gamma_0=2\pi/3\approx 2$. The projection factor of maximum causality, $\gamma_0^{-1}=1$, arises for $\gamma_U\approx 0.235\pi$ as then $\gamma_U=\cos\gamma_U$. The maximum value of γ_0^{-1} is found to be a physical observable instead of a gauge choice. That is, the stereographic projection (from the ambient five-dimensional to the physical four-dimensional spacetime) represents a dynamical embedding map rather than an arbitrary change of coordinates. Because it rescales the lapse function, it modifies the effective g_{tt} experienced by observers confined to the intrinsic hypersurface, giving rise to the apparent acceleration. Details are worked out in Appendix B.

When geodesic equations are applied to the projected time component of the perturbation \hat{h}_{tt} , a fictitious cosmic acceleration of roughly $\gamma_0^{-1}c/t$ emerges in the spatial direction (see Appendix C.3),

$$\frac{|a_{\rm tot} - a_{\rm N}|}{c/t} \approx \frac{1}{\gamma_0} \approx \frac{\cos \gamma_{\rm sys}}{\gamma_{\rm sys}},\tag{2}$$

where $a_N \equiv GM_{\rm sys}(r)/r^2$ is the Newtonian acceleration. However, a time-like component is also found in the acceleration that contributes to the total centrifugal acceleration a_C such that (see Equation (C16) of Appendix C.3)

$$a_C \approx \sqrt{a_N^2 + |a_N| \frac{2c}{\gamma_0 t}},$$
 (3)

which is useful to model galaxy rotation curves under the HMG framework (R. Monjo 2023). Alternatively to Equation (2), the cluster RAR is usually expressed as a quotient between total and Newtonian (spatial) acceleration,

$$\frac{a_{\text{tot}}}{a_{\text{N}}} \approx 1 + \frac{c}{a_{\text{N}} \gamma_0 t},\tag{4}$$

with a factor $\gamma_0^{-1} = \gamma_{\rm sys}^{-1} \cos \gamma_{\rm sys}$, where the projective angle $\gamma_{\rm sys}$ can be estimated from the cluster approach (Equation (C6)) or from the general model (Equation (C4)). To obtain this, we consider the relative geometry (angle) between the Hubble speed $v_{\rm H} \equiv r/t$ and the Newtonian circular speed $v_{\rm N} \equiv \sqrt{GM_{\rm sys}(r)/r}$, which are defined at the radial size r of the (sub)system considered, leading to the following relations for clusters and general systems:

$$\sin^2 \gamma_{\text{clu}}(r) \approx \sin^2 \gamma_{\text{cen}} - (\sin^2 \gamma_{\text{cen}} - \sin^2 \gamma_U)$$

$$\times \frac{2v_{\text{N}}^2(r)}{\varepsilon_{\text{H}}^2 v_{\text{H}}^2(r) + 2v_{\text{N}}^2(r)}$$
(5)

$$\sin^2 \gamma_{\text{sys}}(r) \approx \sin^2 \gamma_U + (\sin^2 \gamma_{\text{cen}} - \sin^2 \gamma_U)$$

$$\times \left| \frac{2v_{\text{N}}^2(r) - \epsilon_{\text{H}}^2 v_{\text{H}}^2(r)}{2v_{\text{N}}^2(r) + \epsilon_{\text{H}}^2 v_{\text{H}}^2(r)} \right|, \tag{6}$$

where $\gamma_{\rm sys}(r)$ is the projective angle of the gravitational system (galaxy or cluster), $\gamma_{\rm cen}$ is the gravitational angle of its central element (black hole or brightest galaxy, respectively),

and the fitting parameter

$$\epsilon_{\mathrm{H}}^{2} \equiv \frac{\rho_{\mathrm{nei}}}{\rho_{\mathrm{vac}}} + \frac{1}{6} \sim \frac{\rho_{\mathrm{nei}}}{\rho_{\mathrm{vac}}} \sim \frac{2v_{\mathrm{N}}^{2}(r_{\mathrm{nei}})}{v_{\mathrm{H}}^{2}(r_{\mathrm{nei}})}$$
(7)

is defined as the relative density of the neighborhood. This is the average density $\rho_{\rm nei} = \rho_{\rm nei}(r_{\rm nei})$ enclosed within radius $r_{\rm nei}$ divided by the cosmic background (vacuum) density $\rho_{\rm vac} \equiv 3/(8\pi Gt^2)$. Note that $\epsilon_{\rm H}^2$ is not constant, as $\rho_{\rm nei}$ depends on r_{nei} . However, the variation between different clusters (or galaxies) is significantly larger than the internal variability within the data range used for each individual system. Therefore, we adopt a zeroth-order approximation (i.e., the first term in the Taylor expansion about a representative value of $\epsilon_{\rm H}^2$) for each gravitational system. Although $\epsilon_{\rm H}^2$ is not a free parameter (as it can be determined from the observed baryonic density), the value of r_{nei} is not available from the data set used, so we estimated the order of magnitude of $\epsilon_{\rm H}$ by fitting galaxy rotation curves. The minimum value of $\epsilon_{\rm H}^2=1/6$ is required for the case with $\nu_{\rm N}=0.$ Thus, the parameter $\epsilon_{\rm H}^{\,2}$ is interpreted as a theoretical point of balance between the orbital speed v_N and Hubble flux v_H (see Appendix C.1 for further information).

To better interpret the parameters $\gamma_{\rm cen}$ and γ_U , it is useful to remember that they correspond to the upper domain of the angular coordinate γ , which is bounded by two extreme conditions:

- 1. the domain of the Universe ($\gamma_U = \pi/3$) when gravitational systems are negligible compared to the Hubble flux (R. Monjo & R. Campoamor-Stursberg 2023) and
- 2. the maximum allowed value of γ is $\gamma_{\rm cen} = \pi/2$, found when the gravitational system is very strong (e.g., in a galaxy center) and therefore it is disconnected from the cosmic expansion (R. Monjo 2023).

Therefore, $\gamma_{\rm cen} \approx \pi/2$ and $\gamma_U \approx \pi/3$ can be fixed here to set a one-parameter ($\epsilon_{\rm H}$) general model from Equation (6). As a second-order approach, this study also assumes that ($\epsilon_{\rm H}$, $\gamma_{\rm cen}$) can be free in our two-parameter model for clusters (Equation (5)).

3. Results and Discussion

3.1. Fitted Values

Individually, fitting of Equation (5) for the quotient between total and Newtonian acceleration (Equation (4)) leads to a square root of the relative density of about $\varepsilon_{\rm H}=38^{+29}_{-11}$ (90% confidence level; Appendix C.4). Using the specific model for clusters (Equation (5)), all fits provide an acceptable χ^2 (p-value < 0.667), except for cluster A2029, which did not pass the χ^2 test for the fixed *neighborhood projective angle* of $\gamma_0=2$ (i.e., $\gamma_U=\pi/3$). However, it did for $\gamma_0=1$ (i.e., $\gamma_U\approx 0.235\pi$), which implies that we need to use the causality limit for the cosmic acceleration instead of the empty-space limit.

Globally, the correlation of RAR values (differences) with respect to the Newton–Hubble speed ratio approach (Equations (2) and (5)) is slightly higher ($R^2=0.83$) than with respect to using the Newtonian acceleration ($R^2=0.79$). The simplest model of fixing $\gamma_U=\pi/3$ and using a single global parameter of $\varepsilon_{\rm H}=40^{+8}_{-6}$ gives a Pearson coefficient of

 $R^2 = 0.75$, while if $\gamma_U = \pi/3$ is replaced by $\gamma_U = 0.235\pi$, we get instead that $R^2 = 0.83$ with $\varepsilon_H = 60^{+20}_{-8}$ (90% confidence level).

Larger anomalies in acceleration are found for the higher orbital speeds in clusters $(\nu_{\rm N}/\nu_{\rm H}\sim\varepsilon_{\rm H}/\sqrt{2})$. However, this is the opposite for galaxies, which experience the maximum anomaly for low orbital velocities $(\nu_{\rm N}/\nu_{\rm H}<\varepsilon_{\rm H}/\sqrt{2})$, as shown in Figure 1. In clusters, the relative density between the dominant brightest cluster galaxy and the neighborhood determines this opposite behavior. The equilibrium value of $\nu_{\rm N}/\nu_{\rm H}\approx\varepsilon_{\rm H}/\sqrt{2}$ points to the transition regime between small and large anomalies, i.e., as small and large proportions of missing gravity using standard physics.

3.2. Predictions for Galaxy and Cluster Dynamics

As discussed in Section 1, HMG derives a relationship between the Milgromian acceleration parameter $a_0 \approx 1.2 \times 10^{-10} \, \mathrm{m \ s^{-2}}$ and the cosmic parameter $c/t \approx 6.9 \times 10^{-10} \, \mathrm{m \ s^{-2}}$, since $a_0 \approx a_{\gamma 0} \equiv 2 \gamma_0^{-1} c/t$ for galaxy rotation curves assuming an approximately constant $\gamma_0^{-1} \approx 0.08$ (R. Monjo 2023). However, the geometry of gravitational systems leads to a variable projection factor $\gamma_0^{-1} \in (0, 1)$, depending on the ratio between Newtonian orbital speed and Hubble flux. This projection factor sets the additional contribution to the apparent acceleration in any given system, which can therefore be larger than the MOND a_0 .

According to the general model of projective angles (Equation (6)), it is expected that galaxies and galaxy clusters exhibit opposite behaviors in their dependence on the speed, but both follow the same theoretical curve. Using $\gamma_{\rm cen}=\pi/2$, $\gamma_U=\pi/3$, and $\varepsilon_{\rm H}=56^{+22}_{-12}$ as obtained from the cluster data, we apply Equations (2) and (6) to predict the behavior of 60 galaxies whose data were collected by S. S. McGaugh et al. (2007). By directly applying Equation (6) to the orbital speed of galaxies, the relative anomaly $(a_{\rm tot}-a_{\rm N})/(c/t)=\gamma_0^{-1}$ is predicted to lie between 0.05 and 0.40, which is close to the value of $\gamma_0^{-1}=0.07^{+0.03}_{-0.02}$ implied by galaxy rotation curves.

The wide range of γ_0^{-1} in clusters depends on the ratio $v_{\rm N}/v_{\rm H}$ between the orbital speed $v_{\rm N}$ and the Hubble flux $v_{\rm H}$, the central projective angle $0.47\pi \lesssim \gamma_{\rm cen} \lesssim 0.50\pi$, and the parameter $\varepsilon_{\rm H} \geqslant 1$. For galaxy rotation curves, this additional dependency is not evident beyond the usual dependence on a_N according to thorough reviews of MOND interpolating functions, showing that γ_0 is almost constant and the actual gravity only depends on the Newtonian acceleration (I. Banik & H. Zhao 2022; R. Stiskalek & H. Desmond 2023). This apparent weakness of the model is easily solved by the fact that an almost constant γ_0^{-1} is obtained from the two-parameter model (Equation (6)) with fitted values of $\gamma_{\rm cen}$ (top left panel of Figure 2). Moreover, the relation of the rotation curve with $v_{\rm N}/v_{\rm H}$ is highly nonlinear as it depends on trigonometric functions. Finally, the correlation between the Newtonian acceleration $a_{\rm N} \propto r^{-2}$ and the flux ratio $v_{\rm N}/v_{\rm H} \propto r^{-3/2}$ is very high for galaxies ($R \approx 0.90$, p-value < 0.001), so the families of interpolating function $f(a_N)$ remove almost all of this nonlinear dependency. In any case, the effective interpolating function of the HMG model is compatible with the best MOND functions (top right panel of Figure 2). It is important to note that HMG predicts the form of the interpolating function, which is arbitrary in MOND and must be found from observations.

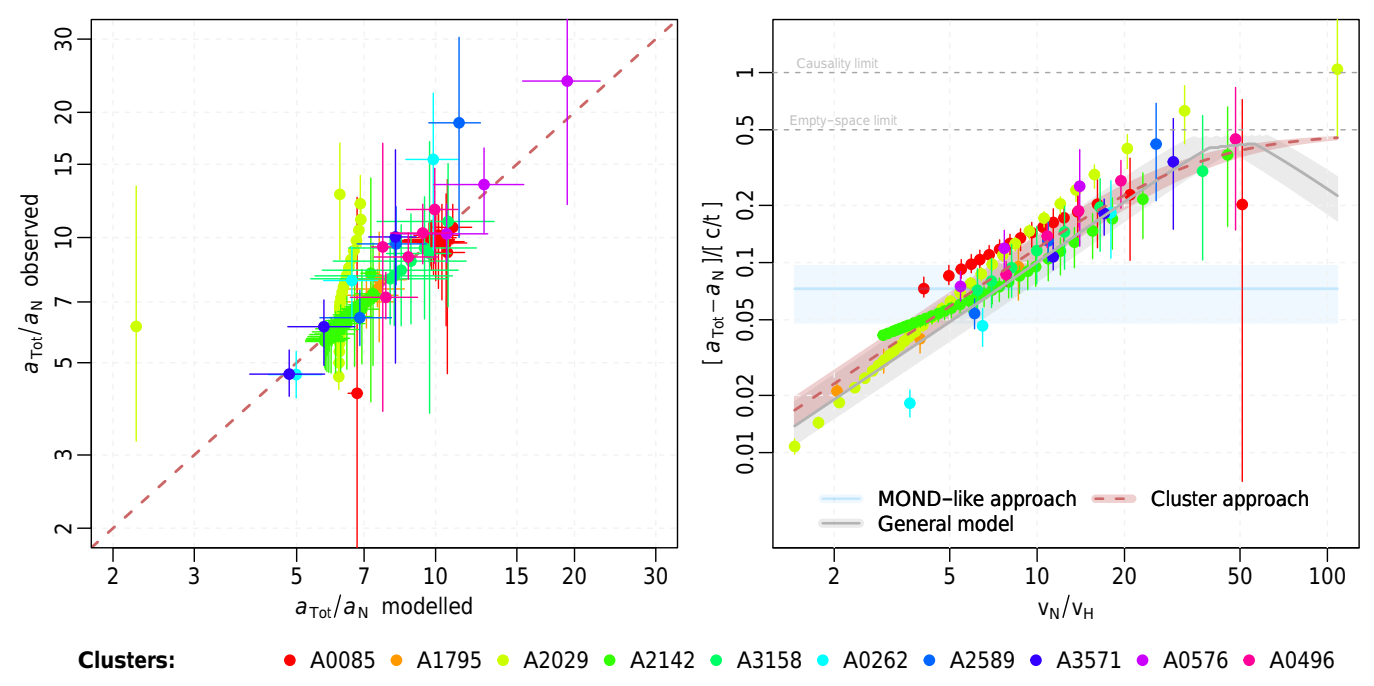


Figure 1. RAR modeling with HMG for the total acceleration (a_{tot}) compared to the Newtonian acceleration (a_N). Left: individual fitting (Equations (4) and (5)) for the galaxy clusters considered (P. Li et al. 2023) using two parameters (ε_H and γ_{cen} ; Table 1). Right: global fitting for all data according to three models: MOND-like constant (blue band), general model (gray band; Equations (2) and (6)), and cluster model (red band; Equations (2) and (5)). The MOND-like model with constant $\gamma_0^{-1} = \gamma_{\text{sys}}^{-1} \cos \gamma_{\text{sys}} \cos \gamma_{\text{sys}}$ was considered with $\gamma_{\text{sys}} = 0.466_{-0.011}^{+0.011} \pi$, which corresponds to Milgrom's constant $a_0 = 2\gamma_0^{-1} c/t = 1.01_{-0.32}^{+0.33} \times 10^{-10} \,\text{m s}^{-2}$ (R. Monjo 2023). In the right panel, both the general model and the specific approach for clusters use only one free parameter (ε_H), done by setting the projective angle of the galaxies to $\gamma_{\text{cen}} = \pi/2$ and $\gamma_U = \pi/3$. The general model (gray band) is represented by $\varepsilon_H = 56_{-12}^{+22}$, while the cluster approach (red band) considers an average of $\varepsilon_H = 40_{-6}^{+8}$, with ε_H being the value of ν_N/ν_H that leads to the maximum RAR anomaly. The shaded areas represent 90% confidence intervals.

After analyzing observations by applying Equation (6) to the galaxy rotation curves with $\gamma_U = \pi/3$, we get a value of $\varepsilon_{\rm H} = 21^{+32}_{-11}$ for $\gamma_{\rm cen} = \pi/2$ while assuming instead that $\gamma_{\rm cen} = 0.48\pi$ gives $\varepsilon_{\rm H} = 18^{+28}_{-10}$. Both are statistically compatible with the cluster-based fitting, which gives $\varepsilon_{\rm H} = 56^{+22}_{-12}$ (bottom left panel of Figure 2). In particular, a value of $\epsilon_{\rm H} \approx 45$ is compatible with both data sets, albeit with a wide variability between the different cases. However, the parameter ε_H is not free at all because there is a significant correlation (R > 0.85, p-value < 0.001) of the form $\varepsilon_{\rm H} \propto \sqrt{\rho(r_{\rm typ})}$ for galactic mass densities $\rho(r_{\rm typ})$ at distances of $r_{\rm typ} \sim 50\text{--}200~{\rm kpc}$ (Appendix C.4 and Figure 5). This gives $\varepsilon_{\rm H} \approx \sqrt{\rho(r_{\rm typ})/\rho_{\rm vac}}$ for the vacuum density $\rho_{\rm vac} = 3/(8\pi G t^2)$, justifying the name of the parameter $\varepsilon_{\rm H}$ as the square root of the relative density of the neighborhood (Equation (C2)). Finally, an empirical relationship (R > 0.80, p-value < 0.001)is also found between $\cos\gamma_{\rm cen}$ and $\log\varepsilon_{\rm H}$ for galaxies, which suggests that the tight range of values of $\gamma_{\rm cen}$ strongly depends on the geometrical features of the gravitational system.

The range of $\epsilon_{\rm H}$ (usually between 10 and 100) ensures that galaxies and clusters show a flat rotation curve that extends out to at least 1 Mpc, which is quite consistent with the extended flat rotation curves around isolated galaxies, as revealed by weak lensing of background galaxies collected from the Kilo-Degree Survey (M. M. Brouwer et al. 2021; T. Mistele et al. 2024). The clusters N5044, N533, A2717, and A2029, with a baryonic mass between $10^{12} \, M_{\odot}$ and $10^{13} \, M_{\odot}$ enclosed within a radius of 1 Mpc (G. W. Angus et al. 2008), produce the following values: (1) an empirical density of $\epsilon_{\rm H} \sim 10$, (2) an acceleration between 10^{-13} and 10^{-11} m s², (3) a Hubble flux $v_{\rm H}$ of about 70 km s⁻¹, and (4) a circular speed $v_{\rm N}$ between 70 and 600 km s⁻¹. These circular speeds at 1 Mpc imply that the

projection factor γ_0^{-1} is between 0.07 and 0.35, producing anomalous accelerations comparable to the Milgromian scale a_0 as $\gamma_0^{-1}=0.08\pm0.01$. The anomaly is noticeably reduced to 0.003 $\leqslant \gamma_0^{-1} \leqslant 0.03$ at 10 Mpc, which is less than half of a_0 .

3.3. Prediction for Small Systems

For small gravitational systems, the orbital velocity v_N is much higher than the Hubble flux v_H , so it is expected that cosmic effects are negligible (with $v_{\rm N}/v_{\rm H} \gg \varepsilon_{\rm H}/\sqrt{2}$). This is because the ratio between the Kepler-Newton speed and the Hubble flux is independent of the size of a spherical system with constant density, but smaller systems tend to be much denser than larger ones. For example, according to Equation (6), an anomaly of only $6.4^{+1.0}_{-0.4}\times10^{-17}\,\mathrm{m~s^{-2}}$ (90% confidence level) is predicted for the solar system at the distance of Pluto's orbit. The predicted anomaly is even smaller for Saturn at 10 au, which is well consistent with the null detection of anomalous effects there from Cassini radio tracking data (A. Hees et al. 2014; H. Desmond et al. 2024). For the Oort cloud, which hypothetically extends between 2 and 200 kau, the predicted anomaly $\Delta a \equiv \gamma_0^{-1} c/t$ increases from $2.2^{+0.4}_{-0.1} \times 10^{-14} \,\mathrm{m \ s^{-2}}$ to $2.3^{+0.4}_{-0.1} \times 10^{-11} \,\mathrm{m \ s^{-2}}$, respectively. The latter value is about 20% of the Milgrom acceleration $a_0 \approx 1.2 \times 10^{-10} \,\mathrm{m \ s^{-2}}$ and could therefore be detected in the future. The most aligned finding is that shown by the work of C. Migaszewski (2023), who suggests that Milgromian gravity could explain the observed anomalies of extreme trans-Neptunian objects and the Oort cloud (2-200 kau, up to 20% of a_N). K. Brown & H. Mathur (2023) claimed that the farthest Kuiper Belt objects (~250 au) also present a MOND signal, but the very detailed orbit integrations

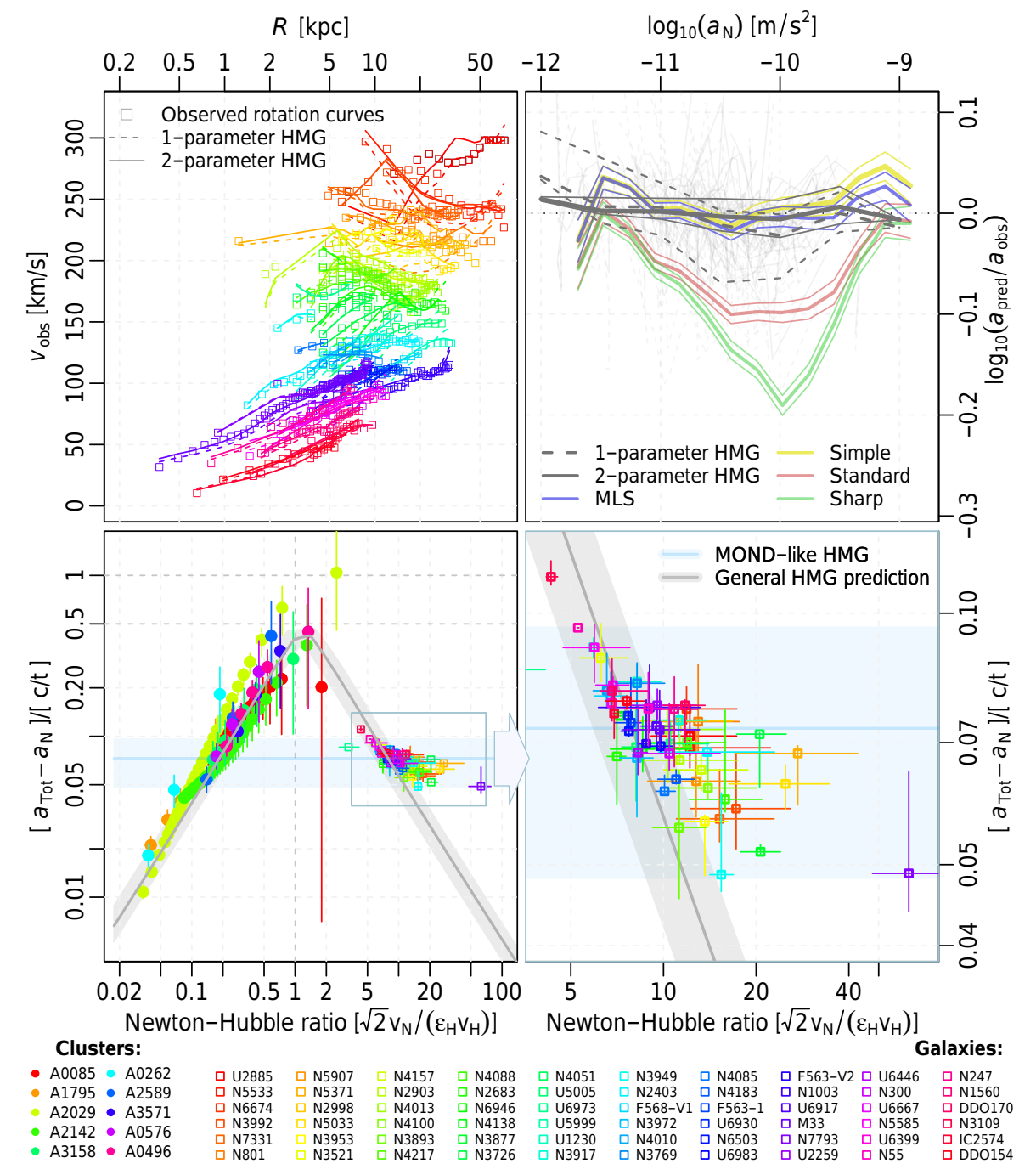


Figure 2. Galaxy rotation curves (squares; S. S. McGaugh et al. 2007) compared with the cluster RAR (circles; P. Li et al. 2023). Top left: fitting of galaxy rotation curves according to the HMG model (Equation (C16); R. Monjo 2023), where γ_0 is modeled by Equation (6) with $\epsilon_{\rm H}$ the only free parameter and $\gamma_{\rm cen}=0.48\pi$ (dashed lines), or with two parameters ($\epsilon_{\rm H}$ and $\gamma_{\rm cen}$; solid lines). Top right: performance of the one-parameter (dashed gray lines) and two-parameter (solid gray lines) model for the ratio of predicted ($a_{\rm pred}$) and observed ($a_{\rm obs}$) centripetal acceleration for the 60 galaxies (light gray lines). Results are compared with the McGaugh-Lelli-Schombert (MLS), simple, standard, and sharp MOND interpolation functions fitted to 153 suitable galaxies. The 1σ confidence intervals for all functions (upper and lower lines of each color) are found as in Figure 23 of I. Banik et al. (2024). Bottom left: global fitting of the data set according to Equations (2) and (6). Bottom right: zoom-in on the theoretical prediction made for galaxies fitted using Equation (6) with $\varepsilon_{\rm H}=21^{+32}_{-11}$. As in Figure 1, the general model prediction for galaxies (gray band) corresponds to the parameter $\varepsilon_{\rm H}=56^{+22}_{-12}$ as an average value of the cluster fitting, with fixed $\gamma_{\rm cen}=\pi/2$ and $\gamma_{\rm U}=\pi/3$. To compare, the MOND-like model and the observational constraint of the general HMG model are also shown, with the shaded area representing the 90% confidence interval. Taking into account that the density of the surrounding system ($\rho_{\rm nei}$) is mainly represented by the fitting parameter $\varepsilon_{\rm H}^2 \sim \rho_{\rm nei}/\rho_{\rm vac} \sim 2v_{\rm N}^2(r_{\rm nei})/v_{\rm H}^2(r_{\rm nei})$ for a certain $r_{\rm nei}$, the interpretation of the abscissa axis (Newton–Hubble ratio) is $\sqrt{2} v_{\rm N}(r)/[\epsilon_{\rm H} v_{\rm H}(r)] \sim [v_{\rm N}(r)/v_{\rm H}(r)]/[\nu_{\rm N}(r_{\rm nei})/v_{\rm H}(r_{\rm nei})]$. Therefore, the abscissa axis represents how far this is from unity, so it is closely related to $v_{\rm N}/v_{$

performed by D. Vokrouhlický et al. (2024) suggest that this interpretation neglects the crucial role of the external field direction rotating as the Sun orbits the Galaxy. Once this is included, it is clear that MOND cannot explain the clustering of

orbital elements presented by the observations. In fact, D. Vokrouhlický et al. (2024) exclude the possible effects of MOND on scales up to about 5–10 kau, which is more consistent with the findings of C. Migaszewski (2023).

Therefore, these findings require further analysis to compare them with the hypothesis of a ninth planet in the trans-Neptunian region (K. Batygin et al. 2024).

In the case of wide binaries, the typical orbital speed at $r \sim 0.1$ pc is about $v_{\rm N} = 350~{\rm m~s^{-1}}$, while the Hubble flux is $v_{\rm H} = r/t \sim 7 \times 10^{-3}~{\rm m~s^{-1}}$. Thus, the Newtonian acceleration is $a_{\rm N} = v_{\rm N}^2/r \sim 4.1 \times 10^{-11}~{\rm m~s^{-2}} < a_0 \approx 1.2 \times 10^{-10}~{\rm m~s^{-2}}$. This is theoretically within the classical MOND regime as $a_{\rm N} < a_0$, leading to an expected 20% enhancement in the Keplerian orbital velocity and thus making wide binaries an important testing ground for MOND (I. Banik & H. Zhao 2018). However, the speed flux is $v_{\rm N}/v_{\rm H} = 5 \times 10^4$, so we expect only a very small anomaly (i.e., a large projective angle $\gamma_{\rm sys}$). Assuming that $\gamma_{\rm cen} = \pi/2$, $\gamma_U = \pi/3$, and a global value of $\varepsilon_{\rm H} = 40^{+30}_{-20}$ in Equation (6), the projective angle $\gamma_{\rm sys} = \pi/2 - 2.20^{+0.14}_{-0.35} \times 10^{-4}\pi$, which corresponds to a projection parameter of $\gamma_0^{-1} = \gamma_{\rm sys}^{-1}\cos\gamma_{\rm sys} = 4.4^{+0.7}_{-0.3} \times 10^{-4}$. The acceleration anomaly would then be $\Delta a \equiv a_{\rm tot} - a_{\rm N} = \gamma_0^{-1} c/t = 3.1^{+0.4}_{-0.2} \times 10^{-13}~{\rm m~s^{-2}}$ (90% interval), that is, a prediction of $2.9 \times 10^{-13}~{\rm m~s^{-2}} < \Delta a < 3.5 \times 10^{-13}~{\rm m~s^{-2}}$ at the 90% confidence level.

Therefore, the acceleration anomalies expected for small systems are less than 1% of the original Milgrom constant $a_0 \approx 1.2 \times 10^{-10} \,\mathrm{m \ s^{-2}}$. This result is consistent with recent comparisons between standard gravity and MOND with data from Gaia wide binary systems (C. Pittordis & W. Sutherland 2019, 2023; I. Banik et al. 2024; S. A. Cookson 2024). However, other authors dispute these results using different data selection criteria and analysis techniques (e.g., X. Hernandez 2023; X. Hernandez et al. 2023; K.-H. Chae 2023, 2024a, 2024b). The wide binary test is still actively debated. For instance, X. Hernandez et al. (2024) and X. Hernandez & P. Kroupa (2025) raise three methodological issues: (i) unrecognized hierarchical triples, (ii) velocity uncertainties due to observational noise, and (iii) insufficient modeling of systematics in statistical inference. Their reanalysis finds evidence for a residual MOND-like signal at projected separations ≥ 0.015 pc, with a clear deviation from Newtonian expectations of about $22\% \pm 8\%$ in the 0.015–0.06 pc range. On the other hand, claims to have detected MOND signals cannot be easily reconciled with Cassini radio tracking data (H. Desmond et al. 2024) and observations of trans-Neptunian objects and long-period comets within the solar system (D. Vokrouhlický et al. 2024). Meanwhile, HMG naturally predicts negligible deviations from Newtonian dynamics in this regime.

3.4. Strengths and Limitations of the Model

The HMG model is not a complete cosmology. Our focus here is on virialized structures and dynamics in the late Universe ($z \lesssim 2$). With a careful comparison to the observed RAR across the full range of probed accelerations in SPARC galaxies and HIFLUGCS galaxy clusters, we show that our two-parameter model is compatible with the latest observations. Moreover, our two parameters are not completely free—they naturally relate to the density of observed matter (Figure 5). This is an advantage because the usual modified gravity theories have difficulty explaining why the RAR differs between galaxies and clusters (e.g., see Figure 5 of P. Li et al. 2023).

Nevertheless, HMG faces some limitations in the early epochs of the Universe because the model distinguishes between extrinsic (linear expansion) and intrinsic (fictitious acceleration) perspectives. In particular, linear expansion cannot explain the observed cosmic microwave background (CMB) power spectrum and Big Bang nucleosynthesis (BBN) due to its very nonstandard timing of key phase transitions, which occur at particular temperatures and thus values of the scale factor (S. Faisal ur Rahman & M. Jawed Igbal 2019; C. Skordis & T. Złośnik 2021; E. Grohs & G. M. Fuller 2022). Altering the timeline by even a single minute could have serious implications for BBN given that free neutrons have a decay time of 15 minutes (R. H. Cyburt et al. 2016; M. Haslbauer et al. 2020; I. Banik & H. Zhao 2022). Therefore, the intrinsic viewpoint of the HMG model needs to address earlier periods in which the expansion history is closer to the standard cosmological model.

According to R. Monjo & R. Campoamor-Stursberg (2023), the apparent cosmic timeline of the intrinsic hyperconical Universe is the same as the standard model, producing a fictitious acceleration compatible with the observed dark energy phenomenology (R. Monjo 2024a, 2024b). In particular, the hyperconical model shows that there exists a unique local solution that produces a fictitious dark energy parameter of $\Omega_{\Lambda} = 2/3$, while global solutions produce $\Omega_{\Lambda} \approx 0.7$. This suggests that the HMG model is promising in later epochs. In future work, we will deeply analyze the ability of the model to reproduce both CMB and BBN observations. The key idea is the dynamical embedding technique in which the linear expansion is actually only in the ambient spacetime as a global time (geometrically, it is the transverse flux of the slicing/foliation on Cauchy surfaces). However, the redshift describes the geodesics of light in the intrinsic metric that presents fictitious acceleration, so its apparent timeline should be the standard one (as described by observers). Therefore, observational tensions arise when trying to work out an apparent expansion history a(t) in the model, i.e., what a latetime observer would actually infer from redshift and luminosity distance or from distance ladder techniques, predicting a Hubble tension (R. Monjo & R. Campoamor-Stursberg 2023).

4. Concluding Remarks

Acceleration is not a geometrical invariant but rather depends on the reference system or framework considered. The hyperconical model (HMG) shows that it is possible to derive local-scale GR to model gravitational systems with anomalous acceleration similar to that attributed to dark matter or dark energy (R. Monjo 2023; R. Monjo & R. Campoamor-Stursberg 2023). Other MOND-based relativistic theories also obtain good performance when modeling galaxy rotation curves with a single global parameter based on acceleration. However, parameters other than acceleration are required because the classical MOND-based RAR does not extend to clusters, and also because recent observations show that gravity is mostly Newtonian on scales smaller than about 10 kau with high precision, even at low acceleration.

This study presents a generalized applicability of the HMG model to a wide range of acceleration anomalies in gravitational systems. Good agreement was obtained with the data collected from 10 galaxy clusters and 60 high-quality galaxy rotation curves. The technique developed for the perturbed metric follows the geometric definition of the sinus of a characteristic angle $\gamma_{\rm sys}$ as a function of the

Newtonian orbital speed $(\nu_{\rm N})$ and the Hubble flux $(\epsilon_{\rm H}\nu_{\rm H})$, i.e., $\sin\gamma_{\rm sys}^2-\sin^2\gamma_U\approx\beta^2(r)|2\nu_{\rm N}^2-\epsilon_{\rm H}^2\nu_{\rm H}^2(r)|$ for $\gamma_U=\pi/3$. The function $\beta(r)$ does not depend on the speeds. It can be fixed by setting two parameters as $\gamma_{\rm sys}=\gamma_{\rm sys}(\gamma_{\rm cen},\ \varepsilon_{\rm H})$. These parameters are a central projective angle $0.47\pi\lesssim\gamma_{\rm cen}\lesssim0.50\pi$ and a relative density $\varepsilon_{\rm H}\geqslant1$.

From the fitting of the general model of $\gamma_{\rm sys}$ (Equation (6)) to the cluster RAR data, an anomaly between 0.05c/t and 0.40c/t is predicted for the galaxy rotation dynamics. This is statistically compatible with the observational estimate of $0.07^{+0.03}_{-0.02}c/t$. As for any modified gravity theory, the challenge was to derive a tight RAR compatible with observations with few free parameters. Classical MOND only has a global free parameter a_0 , but it does not specify the interpolating function, so MOND actually has a lot of freedom to fit observations of galaxy dynamics. In contrast, the HMG model derives a unique interpolation function for rotation curves using only two parameters ($\varepsilon_{\rm H}$, $\gamma_{\rm cen}$) that are not totally free because they are related to the density of matter.

For objects in the outer solar system, such as the farthest Kuiper Belt objects or bodies in the Oort cloud, anomalies between $10^{-14}\,\mathrm{m~s^{-2}}$ and $10^{-11}\,\mathrm{m~s^{-2}}$ are predicted at 1 kau and 100 kau, respectively. Similarly, for wide binary systems, anomalies are expected within the range of 2.9 \times $10^{-13} < \Delta a < 3.5 \times 10^{-13}\,\mathrm{m~s^{-2}}$ (90% confidence level). Such small predicted anomalies imply that local wide binaries should be Newtonian to high precision, as is within the observational limits.

This work provides a chance to falsify a wide range of predictions of a relativistic MOND-like theory that has previously collected successful results in cosmology (R. Monjo 2024b). In future work, we will address other open challenges, especially the modeling of cosmic structure growth and the evolution of early stages of the Universe related to the CMB angular power spectrum and the BBN observations.

Acknowledgments

I.B. is supported by Royal Society University Research Fellowship grant 211046 and was supported by the Science and Technology Facilities Council grant ST/V000861/1. The authors thank Prof. Stacy McGaugh for providing the data for 60 high-quality galaxy rotation curves. The data set corresponding to the 10 galaxy clusters was provided by Prof. Pengfei Li, a kind gesture that we greatly appreciate.

Appendix A Perturbed Vacuum Lagrangian Density

This Appendix summarizes the definition of the local Einstein field equations according to the hyperconical model, that is, by assuming that GR is only valid at local scales (R. Monjo & R. Campoamor-Stursberg 2020; R. Monjo 2024b). In particular, the new Lagrangian density of the Einstein-Hilbert action is obtained by extracting the background scalar curvature $R_{\rm hyp}$ from the total curvature scalar $R \to \Delta R \equiv R - R_{\rm hyp}$ as follows:

$$\mathcal{L} = \frac{1}{16\pi G} \Delta R + \mathcal{L}_M = \frac{1}{16\pi G} \left(R + \frac{6}{t^2} \right) - \rho_M$$
$$= \frac{c^2}{16\pi G} R - \Delta \rho, \tag{A1}$$

where G is the Newtonian constant of gravitation, $R_{\rm hyp}=-6/t^2$ is the curvature scalar of the (empty) hyperconical Universe, $\mathcal{L}_M=-\rho_M$ is the Lagrangian density of classical matter, and $\Delta\rho\equiv\rho_M-\rho_{\rm vac}$ is the density perturbation compared to the "vacuum energy" $\rho_{\rm vac}=3/(8\pi Gt^2)$ with a mass-related event radius $r_{\tilde{M}}\equiv 2G\widetilde{M}\equiv 2G\rho_{\rm vac}\,\frac{4}{3}\pi t^3=t$, where \widetilde{M} is a "total mass" linked to $\rho_{\rm vac}$. Moreover, the orbital velocity $\nu_{\rm N}(\rho_{\rm vac})$ associated with $\rho_{\rm vac}$ at r is given by $2\nu_{\rm N}^2(\rho_{\rm vac})=2G\rho_{\rm vac}\,\frac{4}{3}\pi r^3=r^2/t^2=\nu_{\rm H}^2$. Therefore, a total density ρ_M leads to a total squared orbital velocity $\nu_{\rm N}^2(\rho_M)$ as follows:

$$2v_{\rm N}^{2}(\rho_{M}) = 2G\rho_{M} \frac{4}{3}\pi r^{3} = 2G(\rho_{\rm vac} + \Delta\rho) \frac{4}{3}\pi r^{3}$$
$$= \frac{r^{2}}{r^{2}} + \frac{2GM}{r} = 2v_{\rm N}^{2}(\rho_{\rm vac}) + 2v_{\rm N}^{2}(\Delta\rho), \quad (A2)$$

where we use the definition of $M \equiv \Delta \rho \frac{4}{3}\pi r^3$. Now, let $\theta_M \equiv M/\widetilde{M} \ll 1$ be a (small) constant fraction of energy corresponding to the perturbation $\Delta \rho$, and let $r_M \equiv 2GM = \theta_M t$ be the radius of the mass-related event horizon. Thus,

$$\frac{2GM}{r} = \frac{\theta_M t}{r'^{\frac{t}{t_0}}} = \frac{\theta_M t_0}{r'} = :\frac{2GM_0}{r'}.$$
 (A3)

Therefore, the quotient $M/r = M_0/r'$ is as comoving as $r/t = r'/t_0$.

Moreover, the background metric of the Universe has a Ricci tensor with components $R_{00}^u = 0$ and $R_{ij}^u = \frac{1}{3}R_u g_{ij}$ (R. Monjo 2017; R. Monjo & R. Campoamor-Stursberg 2020). Since $R_{\rm hyp} = -6/t^2$, the Einstein field equations become locally converted to (R. Monjo 2024b)

$$\begin{cases} \kappa P_{00} = \Delta R_{00} - \frac{1}{2} \Delta R g_{00} = R_{00} - \frac{1}{2} R g_{00} - \frac{3}{t^2} g_{00} \\ \kappa P_{ij} = \Delta R_{ij} - \frac{1}{2} \Delta R g_{ij} = R_{ij} - \frac{1}{2} R g_{ij} - \frac{1}{t^2} g_{ij}, \end{cases}$$
(A4)

where $\kappa=8\pi G$ and $P_{\mu\nu}$ are the stress-energy tensor components. Notice that, for small variations in time $\Delta t=t-t_0\ll t_0\equiv 1$, the last terms $(3/t^2)$ and $1/t^2$ are equivalent to consider a "cosmological (almost) constant" or dark energy with equation of state w=-1/3 (varying as a^{-2}).

Appendix B HMG

B.1. Hyperconical Universe and Its Projection

This Appendix reviews the main features of relativistic MOND-like modified gravity derived from the hyperconical model and referred to here as HMG (R. Monjo 2017, 2018, 2023; R. Monjo & R. Campoamor-Stursberg 2020, 2023). Let \mathcal{H}^4 be a (hyperconical) manifold with the following metric:

$$g_{\text{hyp}} \approx dt^2 (1 - kr'^2) - \frac{t^2}{t_0^2} \left(\frac{dr'^2}{1 - kr'^2} + r'^2 d\Sigma^2 \right)$$

$$- \frac{2r'tdr'dt}{t_0^2 \sqrt{1 - kr'^2}},$$
(B1)

where $k=1/t_0^2$ is the spatial curvature for the current value $t_0\equiv 1$ of the age t of the Universe, while $a(t)\equiv t/t_0$ is a linear scale factor, $r'\ll t_0$ is the comoving distance, and Σ represents the angular coordinates. Both the (Ricci) curvature scalar and the Friedmann equations derived for k=1 are locally equivalent to those obtained for a spatially flat $(K_{\rm FLRW}=0)$ $\Lambda{\rm CDM}$ model with linear expansion (R. Monjo & R. Campoamor-Stursberg 2020). In particular, the local curvature scalar at every point $(r'\equiv 0)$ is equal to (R. Monjo 2017)

$$R_{\text{hyp}} = -\frac{6}{t^2} = R_{\text{FLRW}}|_{K=0, a=t/t_0},$$
 (B2)

as for a three-sphere of radius t. This is not accidental because, according to R. Monjo & R. Campoamor-Stursberg (2020), the local conservative condition in dynamical systems only ensures internal consistency for k = 1.

Although Equation (B1) is suitable for use, observers do not directly measure the shift and lapse terms, which produce apparent radial inhomogeneity in the comoving distance (R. Monjo 2017). This spatial inhomogeneity can be assimilated as an equivalent acceleration by applying some "flattening" or spatial projection. The simplest way to remove radial inhomogeneity (and thus measure fictitious acceleration) is to apply a locally conformal projection with radial distortion. In particular, for small regions, a final intrinsic comoving distance \hat{r}' can be defined by an α -distorting stereographic projection (R. Monjo 2018; R. Monjo & R. Campoamor-Stursberg 2023),

$$\begin{cases} r' \mapsto \hat{r}' = \frac{r'}{\left(1 - \frac{\gamma(r')}{\gamma_0}\right)^{\alpha}}, \\ t \mapsto \hat{t} = \frac{t}{1 - \frac{\gamma(r')}{\gamma_0}}, \end{cases}$$
(B3)

where $\gamma = \gamma(r') \equiv \sin^{-1}(r'/t_0)$ is the angular comoving coordinate, $\gamma_0^{-1} \in (0, 1)$ is a projection factor, and $\alpha = 1/2$ is a distortion parameter, which is fixed according to symplectic symmetries (R. Monjo & R. Campoamor-Stursberg 2023). Equation (B3) can be interpreted as a dynamical embedding map rather than an arbitrary change of coordinates. Because it rescales the lapse function, it modifies the effective g_{tt} experienced by observers confined to the intrinsic hypersurface (Equation (B1)), giving rise to an apparent acceleration. Locally, for empty spacetimes, it is expected that $\gamma_0 \approx 2$ (Proposition B.1), which is compatible with the fitted value of $\gamma_0 = 1.6^{+0.4}_{-0.2}$ when Type Ia supernova observations are used (R. Monjo & R. Campoamor-Stursberg 2023). In summary, the projection factor γ_0 depends on a projective angle $\gamma_{\rm sys}$ such that $\gamma_0 = \gamma_{\rm sys}/\cos(\gamma_{\rm sys}) \geqslant 1$, where $\gamma_0 = 2$ corresponds to a total empty projective angle of $\gamma_{\rm sys} \approx \pi/3$, and $\gamma_0 = 1$ is the minimum projection angle allowed by the causality relationship of the arc length $\gamma_0 t_0$. Therefore, the projective angle for an empty or almost empty neighborhood is approximately $\gamma_{\text{nei}} = (0.284 \pm 0.049)\pi \lesssim \pi/3 = : \gamma_U.$

Proposition B.1. Local projection There exists a unique local 1/2-distorting stereographic projection of the hyperconical Universe from its five-dimensional ambient space.

Proof. Let $\lambda \subset \mathbb{R}_{\geqslant 0}$ be a scale factor and let $F_Q: \mathbb{R} \to \mathbb{R}^5$ be a family of 1/2-distorting stereographic projecting beams with $F_Q(\lambda) \in \mathbb{R}^5$ parameterized such as $F_Q(1) = Q(t) = (t, \mathbf{r}, u)$ and $F_Q(0) = Q(0) \equiv (0, \overrightarrow{0}, u_0)$ with $u_0 \equiv -t_0$ and defined as follows:

$$F_{Q} \begin{cases} \hat{t} = t\lambda \\ \hat{r}' = r'\sqrt{\lambda} \\ \hat{u} = u_{0} + (u - u_{0})\lambda \end{cases}$$
 (B4)

This transformation, given by $\mathbf{r}' = r'\mathbf{e}_r = t_0 \sin \gamma \, \mathbf{e}_r \mapsto \hat{r}'\mathbf{e}_r \equiv t_0 \sin \hat{\gamma} \, \mathbf{e}_r$, is performed for the angles $\gamma \mapsto \hat{\gamma}$, preserving the direction \mathbf{e}_r . When the points are projected on the hyperplane $\hat{u} = t_0$, the solution for the distorted stereographic projection is given by some $\lambda = \lambda_s(t, \gamma)$:

$$t_0 = -t_0 + (t\cos\gamma + t_0)\lambda_s \implies \lambda_s(t, \gamma) = \frac{2}{\left(1 + \frac{t}{t_0}\cos\gamma\right)}.$$
(B5)

Expanding the difference between $t < t_0$ and t_0 in terms of the angle γ , it is obtained that

$$\frac{t_0 - t}{t_0} = \gamma + O(\gamma^2) , \qquad (B6)$$

and the projection parameter for $\gamma \ll 1$ approaches

$$\lambda_s(t(\gamma), \gamma) \approx \frac{2}{(1 + (1 - \gamma)\cos\gamma)} \approx \frac{1}{1 - \frac{\gamma}{2}}.$$
 (B7)

Moreover, using the global relationship $t(\gamma)$ proposed by R. Monjo & R. Campoamor-Stursberg (2023) to consider the domain limit given by the angle $\gamma_U = \pi/3$ in empty spaces, the maximum causal difference allowed is $t_0\lambda^{-1} - t \leqslant t_0$; therefore, it can be assumed as follows:

$$\frac{t_0 \lambda^{-1} - t}{t_0} \cos \gamma \approx \frac{\gamma}{\gamma_U} \cos \gamma_U \approx \frac{\gamma}{\gamma_0},$$
 (B8)

with projected angle $\gamma_0 \equiv \frac{\gamma_U}{\cos \gamma_U} = \frac{2}{3}\pi \sim 2$ for empty spaces. Isolating t from the above expression, the scale factor is now

$$\lambda_s \approx \frac{2 - \cos \gamma}{1 - \frac{\gamma}{\gamma_s}} \sim \frac{1}{1 - \frac{\gamma}{\gamma_s}}$$
 (B9)

B.2. Perturbation by Gravitationally Bound Systems

In the case of an (unperturbed) homogeneous Universe, the linear expansion of \mathcal{H}^4 can be expressed in terms of the vacuum energy density $\rho_{\rm vac}(t)=3/(8\pi Gt^2)$, where G is the Newtonian gravitational constant, and thus $\rho_{\rm vac}(t_0)=\rho_{\rm crit}$. That is, one can define an inactive (vacuum) mass or energy $\mathcal{M}(r)=\rho_{\rm vac}\frac{4}{3}\pi r^3$ for a distance equal to r with respect to the reference frame origin. Using the relationship between the coordinate r and the comoving r', the spatial dependence of the

metric is now

$$\frac{r^{2}}{t_{0}^{2}} = \frac{r^{2}}{t^{2}} = \frac{2G\rho_{\text{vac}}\frac{4}{3}\pi r^{3}}{r} = \frac{2G\mathcal{M}(r)}{r} = v_{\text{H}}^{2}(r), \quad (B10)$$

where $v_{\rm H}(r) \equiv r/t$ is the Hubble speed, which coincides with the escape speed of the empty spacetime with vacuum density $\rho_{\rm vac}$.

Definition B.1. Mass of perturbation. A perturbation of the vacuum density $\rho_{\text{vac}} \rightarrow \rho_{\text{M}}(r) \equiv \rho_{\text{vac}} + \Delta \rho$, with an effective density $\Delta \rho$ at r > 0, leads to a system mass $M_{\text{sys}}(r) \equiv \frac{4}{3}\pi r^3 \Delta \rho$ enclosed at a radius r, which is likewise obtained by perturbing the curvature term,

$$\frac{r^2}{t^2} \to \frac{r^2}{t_{\text{sys}}(r)^2} \equiv \frac{r^2}{t^2} + \frac{2GM_{\text{sys}}(r)}{r} = v_{\text{H}}^2(r) + 2v_{\text{N}}^2(r) ,$$
(B11)

with a radius of curvature $t_{sys}(r) \in (2GM_{sys}, t]$, where $v_N(r) \equiv \sqrt{GM_{sys}(r)/r}$ is the classical Kepler–Newton orbital speed (Equation (A2)).

An approximation to the Schwarzschild solution can be obtained in a flat five-dimensional ambient space from the hyperconical metric. For example, let $(t, \mathbf{r}, u) \equiv (t, x, y, z, u) \in \mathbb{R}^{1,4}_{\eta}$ be Cartesian coordinates, including an extra spatial dimension u in the five-dimensional Minkowski plane. As used in hyperconical embedding, $u \equiv t \cos \gamma - t$ is chosen to mix space and time. Now, it includes a gravity field with system mass $M_{\rm sys}$ integrated over a distance \hat{r} such that $\sin^2 \gamma \equiv \frac{r^2}{t^2} \mapsto \frac{\hat{r}^2}{t^2} + \frac{2GM_{\rm sys}}{\hat{r}}$. Notice that r is a coordinate related to the position considered, in contrast to the observed radial distance \hat{r} or its comoving distance $\hat{r}' \equiv (t_0/t)\hat{r}$. With this, the first-order components $\hat{g}_{\mu\nu}$ of the metric perturbed by the mass are

$$\begin{split} \hat{g}_{tt} &= 2\cos\gamma - 1 \approx 1 - \frac{\hat{r}^2}{t^2} - \frac{2GM_{\rm sys}}{\hat{r}}, \\ \hat{g}_{r'r'} &= -\frac{t^2}{t_0^2} \frac{1}{\cos^2\gamma} = -\frac{t^2}{t_0^2} \left(1 - \frac{\hat{r}^2}{t^2} - \frac{2GM_{\rm sys}}{\hat{r}} \right)^{-1} \\ &\approx -\frac{t^2}{t_0^2} \left(1 + \frac{\hat{r}^2}{t^2} + \frac{2GM_{\rm sys}}{\hat{r}} \right), \\ \hat{g}_{r't} &= \frac{t}{t_0} \tan\gamma = \frac{t}{t_0} \frac{\hat{r}}{t} \left(1 - \frac{\hat{r}^2}{t^2} - \frac{2GM_{\rm sys}}{\hat{r}} \right)^{-1/2} \\ &\approx \frac{t}{t_0} \frac{\hat{r}}{t} + O\left(\frac{\hat{r}^3}{2t^3}\right), \\ \hat{g}_{\theta\theta} &= -\frac{t^2}{t^2} \hat{r}'^2, \\ \hat{g}_{\varphi\varphi} &= -\frac{t^2}{t^2} \hat{r}'^2 \sin^2\theta, \end{split}$$

where the hyperconical model is recovered taking $M_{\rm sys}=0$. Therefore, assuming linearized perturbations of the metric $\hat{g}_{\mu\nu}=\hat{g}_{\mu\nu}^{\rm back}+\hat{h}_{\mu\nu}$ with $\hat{g}_{\mu\nu}^{\rm back}\equiv\hat{g}_{\mu\nu}|_{M_{\rm sys}=0}$, we can find a local approach to the Schwarzschild metric perturbation $h|_{\rm Schw}$ as

follows (R. Monjo 2023):

$$\begin{split} \hat{g}_{\text{Schw}} &:\approx [\eta_{\mu\nu} + (\hat{g}_{\mu\nu} - \hat{g}_{\mu\nu}^{\text{back}})] dx^{\mu} dx^{\nu} \\ &\approx \left(1 - \frac{2GM_{\text{sys}}}{\hat{r}}\right) d\hat{r}^2 - \frac{t^2}{t_0^2} \\ &\times \left[\left(1 + \frac{2GM_{\text{sys}}}{\hat{r}}\right) d\hat{r}^{\prime 2} + \hat{r}^{\prime 2} d\Sigma^2\right] \\ &+ \text{neglected shift,} \end{split} \tag{B12}$$

which is also obtained for $\hat{g}_{\mu\nu}$ when $\hat{r}/t \ll 1$, that is, $\lim_{(\hat{r}/t_0) \to 0} [\hat{g}_{\mu\nu}] \approx \hat{g}_{\rm Schw}$. The shift term is neglected in comparison to the other terms, especially for geodesics. Our result is aligned to the Schwarzschild-like metric obtained by A. Mitra (2014) for FLRW metrics, specifically for the case of K=0.

In summary, the first-order approach of the five-dimensionally embedded (four-dimensional) hyperconical metric (Equation (B12)) differs from the Schwarzschild vacuum solution by the scale factor t^2/t_0^2 and a negligible shift term. Therefore, the classical Newtonian limit of GR is also recovered in the hyperconical model, because the largest contribution to gravitational dynamics is given by the temporal component of the metric perturbation h_{tt} . That is, the linearized Schwarzschild geodesics are given by

$$\frac{d^2x^{\mu}}{d\tau^2} \approx \frac{1}{2} \eta^{\mu\nu} \frac{\partial}{\partial x^{\nu}} h_{tt} \left(\frac{dt}{d\tau}\right)^2, \tag{B13}$$

where $\hat{h}_{tt} \approx -2GM_{\rm sys}/\hat{r}$.

Appendix C Modeling Radial Acceleration

C.1. Projective Angles of the Gravitational System

The last Appendix derived a general expression for the anomalous RAR expected for any gravitational system according to the projective angles (which depend on the quotient between orbital speed and Hubble flux) under the hyperconical Universe framework.

From the analysis of perturbations (Equation (B11)), it is expected that any gravitational system (Equation (B12)) results in a characteristic scale $r_{cs}(M_{\rm sys}(r)) \equiv t_{\rm sys}(r)\sin\gamma_{\rm sys}(r)$ given by a projective angle $\gamma_{\rm sys} \in [\pi/3, \pi/2)$ that slightly depends on the radial distance r and the mass $M_{\rm sys}$. Unlike gravitational lensing, a non-null cosmic projection $\gamma_0^{-1} = \gamma_{\rm sys}^{-1}\cos\gamma_{\rm sys} > 0$ is expected for nonconcentrated gravitational systems. In particular, we assume that the maximum projective angle $(\gamma_{\rm sys} = \gamma_{\rm cen} \equiv \pi/2$, minimum cosmic projection) is produced by small, dense, and homogeneous gravitational systems, while the minimum angle $(\gamma_{\rm sys} = \gamma_U \equiv \pi/3$, maximum cosmic projection) corresponds to large systems extended toward an (almost) empty Universe (Figure 3). Since $t_{\rm sys}^2(r) \in (4G^2M_{\rm sys}^2, t^2]$ and $t_{\rm cs}^2(M) \in (4G^2M_{\rm sys}^2, \frac{3}{4}t^2]$, the characteristic scale $t_{\rm cs}^2(M_{\rm sys})$ increases from $t_{\rm cs}^2(M_{\rm sys}) = t_{\rm sys}^2(r) = 4G^2M_{\rm sys}^2 \ll t^2$ up to $t_{\rm cs}^2(M_{\rm sys}) = \frac{3}{4}t_{\rm sys}^2(r) = \frac{3}{4}t^2 = t^2\sin^2\gamma_U$; that is, $t_{\rm sys}^2(r) \in [\frac{3}{4}, 1]$.

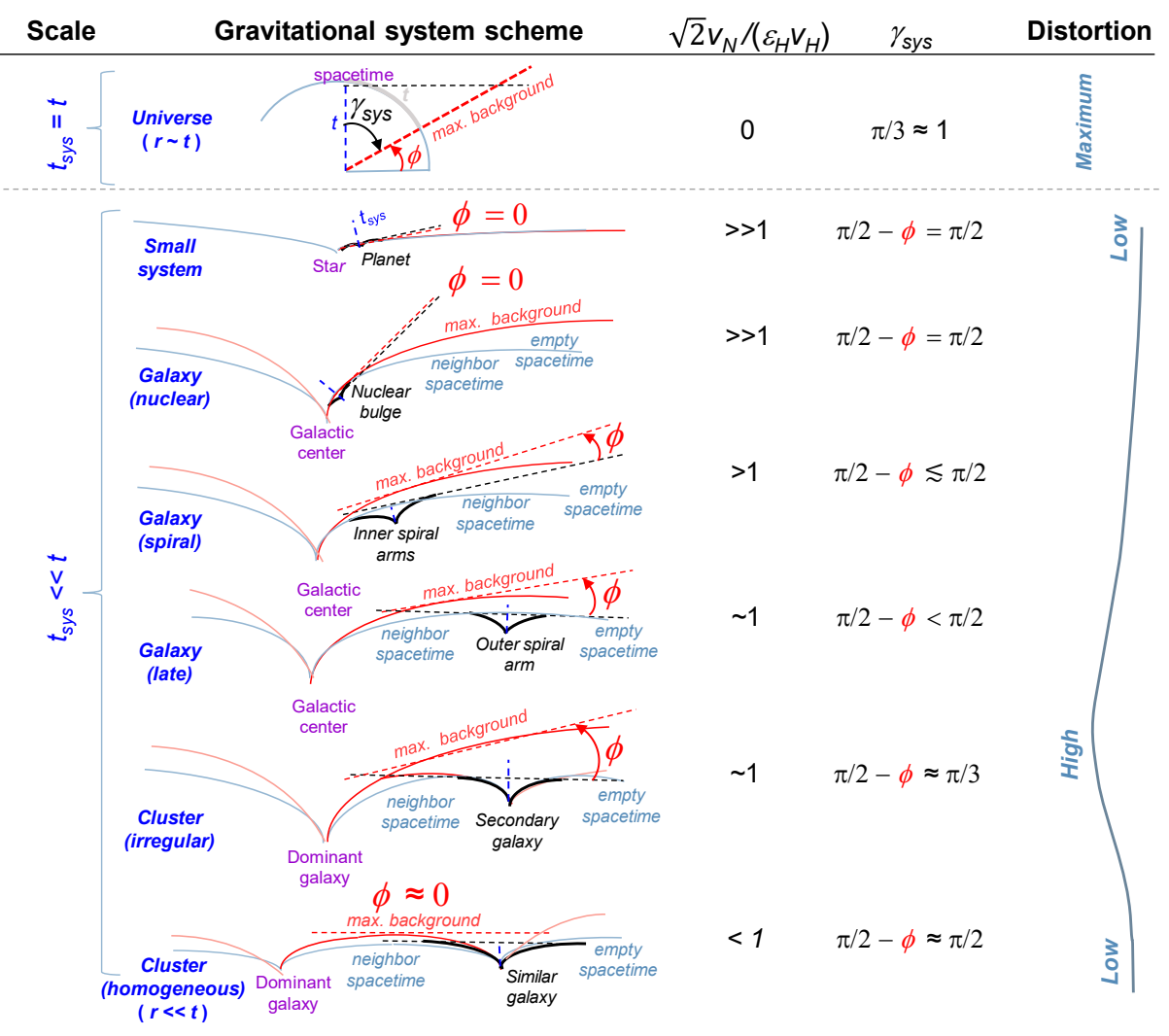


Figure 3. Conceptual model of the projective angle $\gamma_{\rm sys}$ as a function of the relative geometry (orbital speed $v_{\rm N}$ over the Hubble flux $\varepsilon_{\rm H}v_{\rm H}$) for each gravitational system (black curves) with respect to the maximum background spacetime (red curves). To simplify the scheme, the projection factor $\gamma_0^{-1} \equiv \gamma_{\rm sys}^{-1} \cos \gamma_{\rm sys}$ is graphically represented by an auxiliary angle ϕ , defined as the arc between the hyperplane of the gravitational system (dashed black line) and the maximum background hyperplane (dashed red line) curved by the dominant system (purple), such that $\gamma_{\rm sys} = \pi/2 - \phi$. The distance scale r is represented by $t_{\rm sys}$ (Equation (B11)). In addition to the cosmic scale, six gravitational systems are considered: (i) a small system (e.g., solar system), (ii) an early-type galaxy with a dominant nuclear bulge, (iii) a typical spiral galaxy, (iv) a late-type spiral galaxy, (v) an irregular cluster, and (vi) a homogeneous cluster. The dominant objects (purple text) are the star for a small system, the galactic center for galaxies, and the brightest galaxy for a given cluster.

Two definitions are useful for describing the behavior of the characteristic scale r_{cs} . Specifically, let $\gamma_{nei} \equiv \sin^{-1}(r_{cs}/t) \in (0, \gamma_{IJ})$ be the characteristic *neighbor angle*, and let

$$\epsilon_{\rm H}^2 \equiv \frac{\sin^2 \gamma_U}{\sin^2 \gamma_{\rm nei}} - \frac{5}{6} \equiv \frac{\rho_{\rm vac} + \rho_{\rm nei}}{\rho_{\rm vac}} - \frac{5}{6} = \frac{\rho_{\rm nei}}{\rho_{\rm vac}} + \frac{1}{6} \quad (C1)$$

be a *relative density* of the neighborhood matter ($\rho_{\rm nei}$, by definition for a certain radial distance) with respect to the vacuum density $\rho_{\rm vac}=3/(8\pi Gt^2)$. So, Equation (C1) is equivalent to $\frac{5}{6}\sin^2\gamma_{\rm nei}=\sin^2\gamma_U-\epsilon_{\rm H}^2r_{cs}^2/t^2$. The relation of $\gamma_{\rm sys}$ with respect to the gravitational mass

The relation of $\gamma_{\rm sys}$ with respect to the gravitational mass and the scale of speeds can be estimated from the following properties. According to Equation (B11), a gravitational system perturbs the cosmological geometry with a (squared) orbital speed of $v_{\rm N}^2(r) \equiv GM_{\rm sys}(r)/r$ higher than the Hubble expansion speed $v_{\rm H}^2(r) \equiv r^2/t^2$, so the projective angle $\gamma_{\rm sys}$ is

given by

$$\sin^{2} \gamma_{\text{sys}}(r) = \frac{r_{cs}^{2}(M_{\text{sys}})}{r_{\text{sys}}^{2}(r)} = r_{cs}^{2}(M_{\text{sys}}) \left(\frac{1}{t^{2}} + \frac{2GM_{\text{sys}}}{r^{3}}\right)$$

$$= \sin^{2} \gamma_{\text{nei}} + 2\beta^{2}(r)v_{\text{N}}^{2}$$

$$\sim \sin^{2} \gamma_{U} - \beta^{2}(r)\epsilon_{\text{H}}^{2}v_{\text{H}}^{2}(r) + 2\beta^{2}(r)v_{\text{N}}^{2}, \quad (C2)$$

where $\beta^2(r) \equiv r_{cs}^2/r^2 \gg 1$ is an auxiliary function, and Equation (C1) is used. On the other hand, the center of the gravitational system presents a higher density; thus, the cosmic projection should be minimum due to the maximum projective angle $\gamma_{\rm cen} \approx \pi/2$, i.e.,

$$1 \approx \sin^{2} \gamma_{\text{cen}} \approx \frac{r_{cs}^{2}(M_{\text{sys}})}{t_{\text{sys}}^{2}(r)} + 2\epsilon_{\text{H}}^{2} \frac{r_{cs}^{2}(M_{\text{sys}})}{t^{2}}$$
$$\sim \sin^{2} \gamma_{U} + \beta^{2}(r)\epsilon_{\text{H}}^{2} \nu_{\text{H}}^{2} + 2\beta^{2}(r)\nu_{\text{N}}^{2}. \tag{C3}$$

Notice that for the limit when $\sin^2\gamma_{\rm nei}\approx\sin^2\gamma_U=\frac{3}{4}$ or, equivalently, $t_{\rm sys}\approx t$, it is required that $\epsilon_{\rm H}^2\approx\frac{1}{6}$ and $v_{\rm N}\approx 0$. The dependency of $\gamma_{\rm sys}$ on the auxiliary function $\beta(r)$ can be removed by taking the quotient of $\sin^2\gamma_{\rm sys}(r)-\sin^2\gamma_U$ (Equation (C2)) over $\sin^2\gamma_{\rm cen}-\sin^2\gamma_U$ (Equation (C2)). Therefore, it is expected that the projective angle $\gamma_{\rm sys}$ of every gravitational system presents a general relation similar to

$$\frac{\sin^{2} \gamma_{\text{sys}}(r) - \sin^{2} \gamma_{U}}{\sin^{2} \gamma_{\text{cen}} - \sin^{2} \gamma_{U}} \sim \left| \frac{2v_{\text{N}}^{2}(r) - \epsilon_{\text{H}}^{2} v_{\text{H}}^{2}(r)}{2v_{\text{N}}^{2}(r) + \epsilon_{\text{H}}^{2} v_{\text{H}}^{2}(r)} \right|, \quad (C4)$$

with two free parameters, $\epsilon_{\rm H} \geqslant \frac{1}{6}$ and $\gamma_{\rm cen} \approx \pi/2$. Notice that the maximum projective angle (i.e., $\gamma_{\rm sys} = \gamma_U$) is found when the gravitational and Hubble fluxes are in equilibrium, modulated by the parameter $\epsilon_{\rm H}$. On the other side, for galaxies and small gravitational systems, the Kepler–Newton orbital speed $v_{\rm N}^2$ is much larger than the Hubble flux. Thus, the projective angle $\gamma_{\rm sys}(r) \equiv \gamma_{\rm gal}(r)$ can be estimated by the following galactic relation (R. Monjo 2023):

$$\frac{\sin^2 \gamma_{\rm sys}(r) - \sin^2 \gamma_{\rm nei}}{\sin^2 \gamma_{\rm cen} - \sin^2 \gamma_U} \sim \frac{2\nu_{\rm N}^2(r)}{2\nu_{\rm N}^2(r) + \epsilon_{\rm H}^2 \nu_{\rm H}^2(r)}, \quad (C5)$$

with $\gamma_{\rm nei} \sim \gamma_U \approx \pi/3$ and one free parameter, which is $\epsilon_{\rm H}^2 \gtrsim 1$ if $\gamma_{\rm cen} = \pi/2$ is fixed or $\gamma_{\rm cen} \lesssim \pi/2$ if $\epsilon_{\rm H} = 1$ is fixed. Thus, two limiting cases are $\sin \gamma_{\rm sys} \approx 1 \Rightarrow \gamma_{\rm sys} \approx \pi/2$ when the orbital speed is $v_{\rm N}(r) \gg \varepsilon_{\rm H} v_{\rm H}(r)$, while $\sin \gamma_{\rm sys} \approx \frac{\sqrt{3}}{2} \Rightarrow \gamma_{\rm sys} \approx \pi/3$ when the orbital speed is $v_{\rm N}(r) \ll \varepsilon_{\rm H} v_{\rm H}(r)$, which is the lower limit of the neighborhood projective angle $(\gamma_{\rm nei})$.

On the other hand, radial accelerations (without regular orbits) of large-scale objects such as galaxy clusters are expected to present opposite behavior with respect to Equation (C5), since the gravitational center is not a galactic black hole but is close to a dominant galaxy (the brightest cluster galaxy; R. De Propris et al. 2020; D. Shi et al. 2024), and the neighborhood now corresponds to the large-scale environment of the clusters themselves. Therefore, the projective angle $\gamma_{\rm sys}$ of the largest structures is approximated by the following cluster relation:

$$\frac{\sin^2 \gamma_{\rm cen} - \sin^2 \gamma_{\rm sys}(r)}{\sin^2 \gamma_{\rm cen} - \sin^2 \gamma_U} \sim \frac{2\nu_{\rm N}^2(r)}{2\nu_{\rm N}^2(r) + \epsilon_{\rm H}^2 \nu_{\rm H}^2(r)}, \quad (C6)$$

where $v_{\rm N}^2(r)$ is the orbital speed profile of the cluster and $\gamma_{\rm cen} \lesssim \pi/2$ is the averaged projective angle for its central object; now we expect that the projective angle for clusters is a variable $\gamma_{\rm sys}(r) \in [\pi/3, \pi/2)$ but close to the neighborhood value $\gamma_{\rm nei} \sim \gamma_U = \pi/3$.

However, a perfectly homogeneous distribution of low-density galaxies in a cluster will lead to a balance between the different galaxies that form it, so the cluster radial acceleration will be approximately zero ($\nu_{\rm N}\sim0$) and anomalies are not expected. Thus, the projective angle will be $\gamma_{\rm sys}\approx\pi/2$ for both Equations (C4) and (C6); that is, no significant geometrical differences are expected between the external and internal parts of the cluster (see the last case of Figure 3). Conversely, for irregular clusters ($\nu_{\rm N}\sim\epsilon_{\rm H}\nu_{\rm H}$ with $\epsilon_{\rm H}\gg1$ in Equation (C4) or $2\nu_{\rm N}^2\gtrsim\epsilon_{\rm H}^2\nu_{\rm H}^2(r)$ in Equation (C6)), the radial acceleration will be very similar to the cosmic expansion (with

angle $\gamma_{\rm sys} = \gamma_U = \pi/3$). Notice that, for very inhomogeneous systems ($\nu_{\rm N} \gg \epsilon_{\rm H}\nu_{\rm H}$), Equation (C4) recovers the behavior of high-density galaxies (Equation (C5)) with $\gamma_{\rm sys}(r) = \gamma_{\rm gal}(r)$. Moreover, for $2\nu_{\rm N}^2 \in (0, \ \epsilon_{\rm H}^2\nu_{\rm H}^2)$, Equation (C4) behaves in a similar way as in Equation (C6), as expected.

C.2. Cosmological Projection of the Schwarzschild Metric

Henceforth, the constant of light speed $c \equiv 1$ will not be omitted from the equations so we can compare with real observations later. Let λ be the scaling factor of an α -distorting stereographic projection (Equation (B3)) of the coordinates $(r', u) = (ct \sin \gamma, ct \cos \gamma) \in \mathbb{R}^2$, used to simplify the spatial coordinates $(r', u) \in \mathbb{R}^4$ due to angular symmetry. For nonempty matter densities, we contend that $\gamma_{\rm sys}$ depends on the orbital speed of the gravity system considered. However, the first-order projection can be performed by assuming that the dependence on distances is weak (i.e., with $\gamma_0^{-1} = \gamma_{\rm sys}^{-1} \cos \gamma_{\rm sys}$ being approximately constant for each case). Thus, the stereographic projection is given by the scale factor λ such as (see, for instance, R. Monjo 2023; R. Monjo & R. Campoamor-Stursberg 2023)

$$\lambda = \frac{1}{1 - \frac{\gamma}{\gamma_0}} \approx 1 + \frac{r'}{\gamma_0 t_0 c} \,, \tag{C7}$$

where $\gamma = \sin^{-1}[r'/(t_0c)] \approx r'/(t_0c)$ is the angular position of the comoving distance $r' = (t_0/t) r$. Therefore, the projected coordinates are

$$\begin{cases} \hat{r}' = \lambda^{\alpha} r' \approx \left(1 + \frac{\alpha r'}{\gamma_0 t_0 c}\right) r', \\ \hat{t} = \lambda t \approx \left(1 + \frac{r'}{\gamma_0 t_0 c}\right) t. \end{cases}$$
 (C8)

At a local scale, the value of $\alpha=1/2$ is required to guarantee consistency in dynamical systems (R. Monjo & R. Campoamor-Stursberg 2023), but the parameter α is not essential in this work, since only the temporal coordinate is used in our approach below.

Applying this projection to the perturbed metric (Equation (B12)) and obtaining the corresponding geodesics, it is easy to find a first-order approach of the cosmic contribution to modify the Newtonian dynamics in the classical limit, as shown below (Section C.3).

C.3. First-order Perturbed Geodesics

Assuming that the projection factor $\gamma_0^{-1} = \gamma_{\rm sys}^{-1} \cos \gamma_{\rm sys}$ is approximately constant, the quadratic form of the projected time coordinate (Equation (C8)) is as follows:

$$d\hat{t}^2 \approx \left(1 + \frac{2r'}{\gamma_0 t_0 c} + \frac{2t \dot{r}'}{\gamma_0 t_0 c}\right) dt^2 + \text{higher-order terms.}$$
 (C9)

By using these prescriptions, our Schwarzschild metric (Equation (B12)) is expressed in projected coordinates (\hat{t}, \hat{r}') or in terms of the original ones (t, r'); that is,

 $\hat{g}_{\text{Schw}} = \hat{g}_{\mu\nu} d\hat{x}^{\mu} d\hat{x}^{\nu} = g_{\mu\nu} dx^{\mu} dx^{\nu}$, with

$$\hat{g}_{\text{Schw}} \approx \left(1 - \frac{2GM_{\text{sys}}(\hat{r})}{c^2 \hat{r}}\right) c^2 d\hat{t}^2 - \frac{\hat{t}^2}{t_0^2} \,\hat{r}'^2 d\Sigma^2$$

$$\approx g_{tt} c^2 dt^2 + g_{ii} (dx^i)^2. \tag{C10}$$

Finally, this is locally expanded up to first-order perturbations in terms of γ_0 . Notice that, according to Equation (B12), the background terms r'^2/t_0^2 do not produce gravitational effects, and thus they can be neglected. Here, one identifies a projected perturbation h_{tt} of the temporal component of the metric, $g_{tt} = \eta_{tt} + h_{tt} = 1 + h_{tt}$, with $\eta_{\mu\nu} = \eta^{\mu\nu} = \text{diag}(1, -1, -1, -1)$. Thus, if M_{sys} is assumed to be mostly concentrated in the central region of the gravitational system, the first-order perturbation of the temporal component of the metric is

$$h_{tt} \approx -\frac{2GM_{\rm sys}(r)}{rc^2} \left(1 - \frac{\alpha r}{\gamma_0 tc}\right) + \frac{2}{\gamma_0 c} \left(\frac{r}{t} + \frac{t}{t_0} \dot{r}'\right), \quad (C11)$$

where the spatial projection $\hat{r} \approx (1 + \alpha r/(\gamma_0 ct)) r$ is considered (from Equation (C8)), and the relation between comoving distance r' and spatial coordinate r is also used $(r'/t_0 = r/t)$.

Under the Newtonian limit of GR, the largest contribution to gravity dynamics is given by the temporal component of the metric perturbation h_{tt} . That is, Schwarzschild geodesics (Equation (B13)) produce both time-like and space-like acceleration components from the metric perturbation h_{tt} ,

$$\frac{d^2\hat{s}}{c^2dt^2} \approx \frac{1}{2} \frac{\partial}{\partial x^0} h_{tt} e_t - \frac{1}{2} \frac{\partial}{\partial x^i} h_{tt} e_i = :a^t e_t + a^i e_i, \quad (C12)$$

where the four-position $\hat{s} \equiv (c\Delta t, x^i) = c\Delta t \ e_t + x^i \ e_i = : c\Delta t + x \in \mathbf{R}^{1,3}$ is assumed, with canonical basis $\{e_t, e_1, e_2, e_3\}$ and dual basis $\{e^t, e^1, e^2, e^3\}$. For a freely falling particle with central-mass reference coordinates $\mathbf{x} = x^i e_i = (r, 0, 0) = \mathbf{r} \in \mathbb{R}^3$, it experiences an acceleration of about

$$\frac{d^2\hat{s}}{dt^2} = a^t e_t + a^r e_r \approx \left(\frac{\dot{r}'}{t_0} - \frac{r + \frac{1}{2}\alpha r_M}{\gamma_0 t^2}\right) e_t - \left(\frac{GM_{\text{sys}}}{r^2} + \frac{c}{\gamma_0 t}\right) \frac{r}{r}$$

$$\approx a_N - \frac{c}{\gamma_0 t} \frac{r}{r} - \frac{r}{\gamma_0 t^2} e_t, \tag{C13}$$

where $r_M \equiv 2GM_{\rm sys}/c^2 \ll r$ is the Schwarzschild radius, which is neglected compared to the spatial position r. That is, an acceleration anomaly is obtained mainly in the spatial direction, about $|\mathbf{a} - a_{\rm N}| \approx \gamma_0^{-1} c/t$ for $\mathbf{a} \equiv a^r e_r$. However, the total acceleration also has a time-like component, that is, in the direction e_r . In particular, for a circular orbit with radius r, and taking into account the nonzero temporal contribution to the acceleration in the hyperconical Universe with radius ct

(R. Monjo 2023), the total centrifugal acceleration is

$$\frac{v^2}{c^2}e_s = -(cte_te^t + x^ie_ie^i)\frac{d^2\hat{s}}{c^2dt^2} \approx ct\left(\frac{r}{\gamma_0c^2t^2}\right)e_t + \left(\frac{GM_{\text{sys}}}{c^2r^2} + \frac{1}{\gamma_0ct}\right)\frac{x^ix_i}{r}e_i, \tag{C14}$$

where e_s is an effective space-like direction $(||e_s||^2 = e_s e^s = -1)$, while the absolute value of the velocity is given by

$$\frac{v^{4}}{c^{4}} = -\left|\left|\frac{v^{2}}{c^{2}}e_{s}\right|\right|^{2} \approx \left(\frac{GM_{\text{sys}}}{rc^{2}}\right)^{2} + \frac{2GM_{\text{sys}}}{\gamma_{0}tc^{3}}$$

$$\Rightarrow \begin{cases}
v \approx \sqrt{\frac{GM_{\text{sys}}}{r}}, & \text{if } \frac{GM_{\text{sys}}}{r^{2}} \gg \frac{2c}{\gamma_{0}t} = :a_{\gamma 0}, \\
v \approx \sqrt{\frac{2GM_{\text{sys}}c}{\gamma_{0}t}}, & \text{if } \frac{GM_{\text{sys}}}{r^{2}} \ll \frac{2c}{\gamma_{0}t} = a_{\gamma 0},
\end{cases} (C15)$$

which satisfies two well-known limits of Newtonian and Milgromian dynamics (Equation (C15) right), where a_0 is Milgrom's acceleration parameter and $M_{\rm sys}=M_{\rm sys}(r)$ is the total mass within the central sphere of radius r. Finally, the velocity curve v=v(r) can be reworded in terms of the Newtonian circular speed $v_{\rm N} \equiv \sqrt{GM_{\rm sys}(r)/r}$. Therefore, the predicted MDAR for rotation curves is

$$\left(\frac{v}{v_{\rm N}}\right)^2 \approx \sqrt{1 + \frac{1}{|a_{\rm N}|} \frac{2c}{\gamma_0 t}} \Rightarrow \frac{a_C}{a_{\rm N}} \approx \sqrt{1 + \frac{1}{|a_{\rm N}|} \frac{2c}{\gamma_0 t}},\tag{C16}$$

where $a_C = v^2/r$ is the total radial acceleration and $a_N = GM_{\rm sys}/r^2$ is the Newtonian acceleration. However, the absence of rotation in galaxy clusters leads to a radial acceleration similar to Equation (C13). In any case, the projection factor $\gamma_0^{-1} = \gamma_{\rm sys}^{-1} \cos \gamma_{\rm sys}$ depends on the projective angle $\gamma_{\rm sys}$, which can be estimated from the galaxy cluster approach (Equation (C6)) or the general model (Equation (C4)), respectively, as follows:

$$\sin^2 \gamma_{\text{clu}}(r) \approx \sin^2 \gamma_{\text{cen}} - (\sin^2 \gamma_{\text{cen}} - \sin^2 \gamma_U) \frac{2v_N^2(r)}{2v_N^2(r) + \varepsilon_H^2 v_H^2(r)}, \quad (C17)$$

$$\sin^2 \gamma_{\text{sys}}(r) \approx \sin^2 \gamma_U + (\sin^2 \gamma_{\text{cen}} - \sin^2 \gamma_U)$$

$$\left| \frac{2\nu_{\text{N}}^2(r) - \epsilon_{\text{H}}^2 \nu_{\text{H}}^2(r)}{2\nu_{\text{N}}^2(r) + \epsilon_{\text{H}}^2 \nu_{\text{H}}^2(r)} \right|, \quad (C18)$$

where $\gamma_{\rm cen}$ can be fixed to $\gamma_{\rm cen} = \pi/2$ to test the one-parameter $(\epsilon_{\rm H})$ general model of Equation (C18), while this study assumes that $\{\epsilon_{\rm H}, \gamma_{\rm cen}\}$ are free in our two-parameter model for clusters (Equation (C18)). Finally, the empty projective angle is usually set as $\gamma_U = \pi/3$ (R. Monjo &

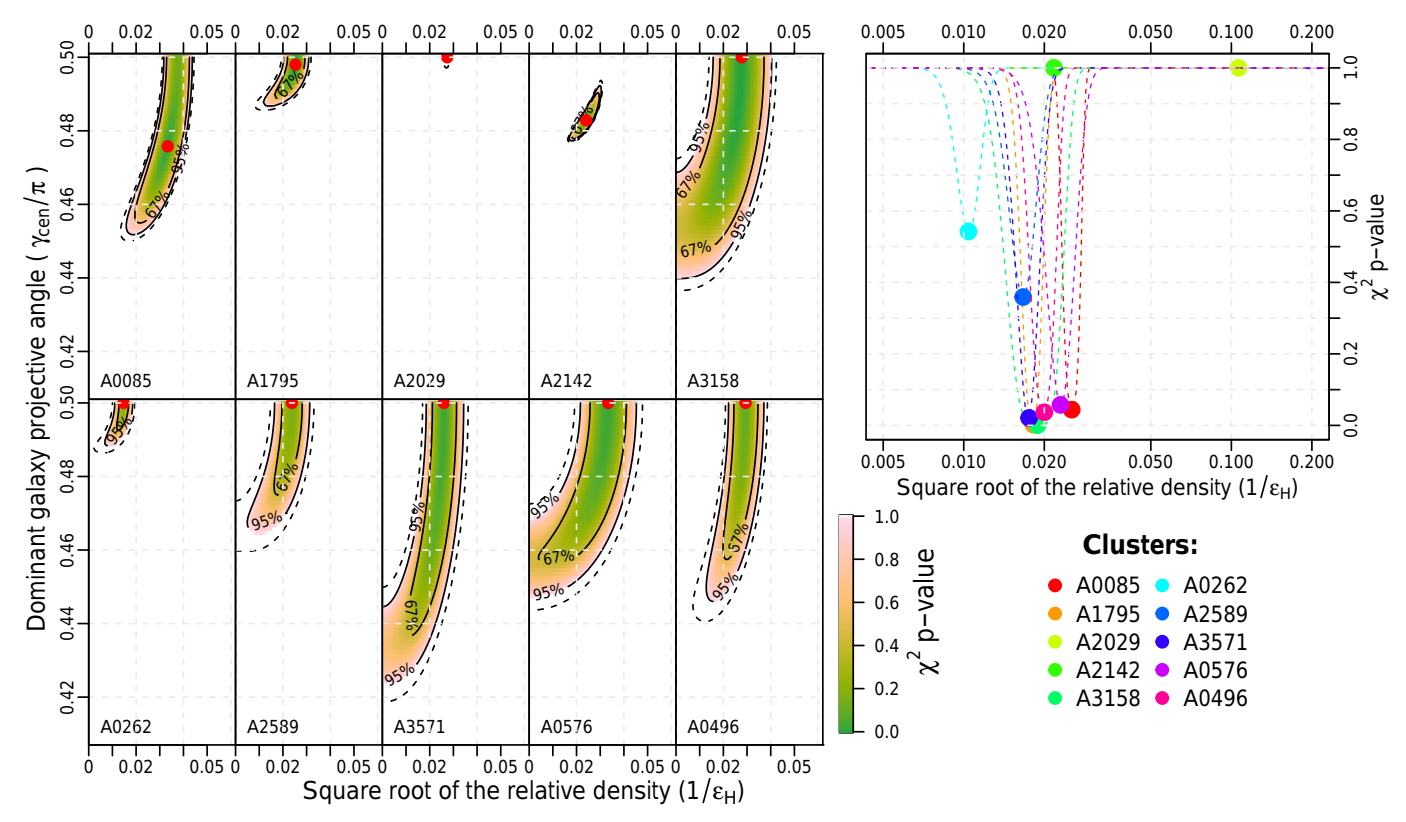


Figure 4. Observational constraints on the proposed models fitted to RAR data of the 10 galaxy clusters considered (P. Li et al. 2023). Left: best values (red points) and uncertainty area (green shaded regions showing the 1σ confidence level) of the two parameters ($\varepsilon_{\rm H}$ and $\gamma_{\rm cen}$; see Table 1) used in fits to individual clusters according to the specific approach (Equation (C17) is used in Equation (C13)). Right: best fit of the single free parameter ($\varepsilon_{\rm H}$) used in the general model (Equation (C18) used in Equation (C13)), with fixed $\gamma_{\rm cen} = 0.48\pi$. In both cases (one or two free parameters), the *projective angle of the neighborhood* (γ_U) was fixed to $\gamma_U = \pi/3$. Notice that cluster A2029 did not pass the χ^2 test even with the two-parameter model. However, it passed the test for $\gamma_U = 0.235\pi$, corresponding to $\gamma_U^{-1} \cos \gamma_U \approx 1$.

R. Campoamor-Stursberg 2023), which produces a projection factor of $\gamma_U^{-1}\cos\gamma_U\approx 1/2$.

C.4. Individual Fitting

Observed data on the RAR of 10 clusters (0.0328 < z < 0.0899) were collected from the study performed by P. Li et al. (2023). Individually, fitting of Equation (C17) for the anomaly between the total spatial acceleration and Newtonian acceleration (Equation (C13)) leads to a square root of the relative density of about $\varepsilon_{\rm H}=38^{+29}_{-11}$ (90% confidence level; Figure 4). All these results are obtained by fixing the constants $\gamma_U=\pi/3$ and $\gamma_{\rm cen}=\pi/2$. The general model (Equation (C18)), with only one free parameter ($\varepsilon_{\rm H}$), gave good results for 8 of the 10 clusters, showing difficulties in fitting the more available data from the A2029 and A2142 clusters (Table 1). If two parameters are considered ($\varepsilon_{\rm H}$, $\gamma_{\rm cen}$), the results considerably improve, except for the A2029 cluster, which requires changing $\gamma_U^{-1}\cos\gamma_U \rightarrow 1$ to be compatibly fitted to the observations.

The same two-parameter ($\varepsilon_{\rm H}$, $\gamma_{\rm cen}$) general model (Equation (C18) with $\gamma_U=\pi/3$) was also applied to the 60 high-quality galaxy rotation curves, obtaining an acceptable result for all of them. The case of one parameter ($\varepsilon_{\rm H}$ free when $\gamma_{\rm cen}=0.48\pi$ is set) showed a slightly larger chi-square statistic and p-value, but these are also acceptable for all of them. Moreover, an empirical relationship between the single parameter $\epsilon_{\rm H}$ and the square root of a relative density is found, which approximately defines an identity $\epsilon_{\rm H}^2\cong \rho(r_{\rm typ})/\rho_{\rm vac}$ in units of

Table 1
Fitting Parameters for the Clusters

Name (Data)	General Model		Specific Model for Clusters		
	$\varepsilon_{ m H}$	χ^2 p-val.	$\varepsilon_{ m H}$	$\gamma_{\rm cen}/\pi$	χ^2 p-val.
A0085 (17)	40+6	0.04	31^{+5}_{-4}	$0.474^{+0.017}_{-0.009}$	< 0.01
A1795 (4)	55^{+14}_{-9}	< 0.01	39^{+6}_{-4}	$0.499^{+0.001}_{-0.006}$	< 0.01
A2029 (32)	52^{+40}_{-20}	>0.95	37^{+15}_{-10}	$0.500^{+0}_{-0.002}$	>0.95
A2142 (31)	46^{+15}_{-15}	>0.95	41^{+4}_{-2}	$0.483^{+0.003}_{-0.002}$	< 0.01
A3158 (7)	53^{+39}_{-17}	< 0.01	37^{+18}_{-8}	$0.491^{+0.009}_{-0.030}$	< 0.01
A0262 (3)	96^{+32}_{-19}	0.54	67^{+10}_{-6}	$0.500^{+0}_{-0.005}$	0.57
A2589 (3)	60^{+37}_{-14}	0.36	41^{+10}_{-4}	$0.500^{+0}_{-0.013}$	0.47
A3571 (3)	57^{+22}_{-12}	0.02	39^{+8}_{-6}	$0.495^{+0.005}_{-0.036}$	0.14
A0576 (3)	44^{+22}_{-11}	0.06	31^{+8}_{-6}	$0.493^{+0.007}_{-0.023}$	0.13
A0496 (5)	50^{+16}_{-9}	0.04	33^{+6}_{-4}	$0.500^{+0}_{-0.028}$	0.14

Note. Individual fitting of Equation (5) to each cluster according to the general model (Equation (6)) with one parameter (ε) and with the specific model for clusters (Equation (5) with two parameters, namely, ε and $\gamma_{\rm cen}$). The p-value is given for the lowest χ^2 .

vacuum density $\rho_{\rm vac} \equiv 3/(8\pi Gt^2)$ for an observed density $\rho(r_{\rm typ})$ that is defined at a *typical neighborhood* distance of approximately 4 times the maximum radius $(r_{\rm typ} \approx 4 \times r_{\rm max})$, fitted at R=0.85, p-value <0.0001; Figure 5, left) for each galaxy rotation curve and equal to the minimum radius $(r_{\rm typ} \approx r_{\rm min})$ for the data of each cluster. This *typical distance* corresponds to $r_{\rm typ} \approx 50$ –200 kpc. A more general empirical relationship is

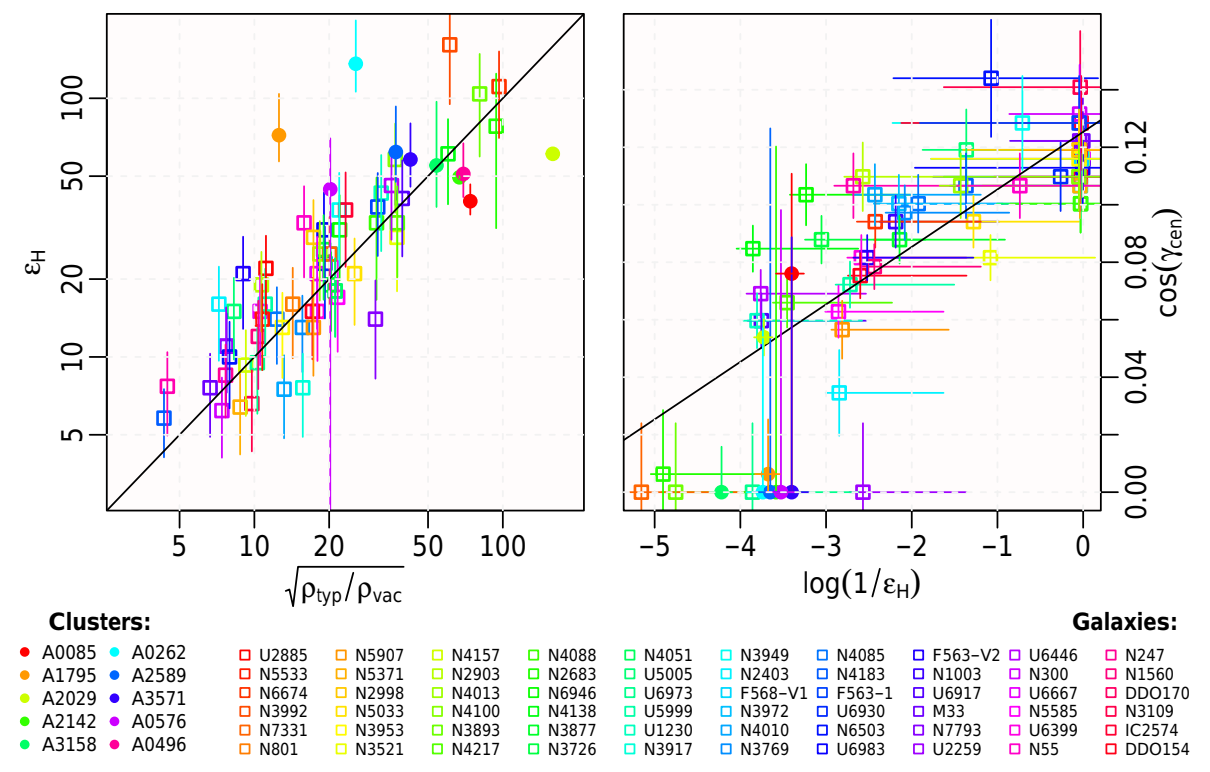


Figure 5. Model parameters fitted to the 60 high-quality galaxy rotation curves (squares), empirical relationships (black lines), and comparison with the fitting to the RAR data of 10 clusters (circles). Left: constraint on the one-parameter HMG model for galaxies, with fixed $\gamma_{\rm cen} = 0.48\pi$ and free $\varepsilon_{\rm H}$. This shows an (almost) empirical identity between the single parameter $\epsilon_{\rm H}$ and the square root of the relative density $\rho_{\rm typ}/\rho_{\rm vac}$. In other words, in units of vacuum density $\rho_{\rm vac} \equiv 3/(8\pi G t^2)$, an observed density $\rho_{\rm typ} \equiv \rho(r_{\rm typ})$ is defined at a typical equilibrium distance of $r_{\rm typ} \sim 50-200$ kpc, whose fit has been found (R = 0.85, p-value < 0.0001) as 4 times the maximum radius ($r_{\rm typ} \approx 4 r_{\rm max}$) for each galaxy rotation curve and equal to the minimum radius ($r_{\rm typ} \approx r_{\rm min}$) for the data of each cluster. Right: constraint on the two-parameter HMG model for galaxies, which shows a relationship between $\epsilon_{\rm H}$ and $\gamma_{\rm cen}$ such that $\cos(\gamma_{\rm cen}) = \cos(0.460\pi) - 0.020 \ln \varepsilon_{\rm H}$ for $1 \le \varepsilon_{\rm H} < 400$, with a Pearson coefficient of R = 0.80 (p-value < 0.0001; black regression line).

found for $\epsilon_{\rm H}^2 - \frac{1}{6} = (\rho(r_{\rm typ})/\rho_{\rm vac})^{\zeta}$ with $\zeta = 0.92^{+0.08}_{-0.12}$ (R = 0.86, p-value < 0.0001).

Finally, when the two-parameter HMG model is considered for galaxies, an additional relationship is found between ϵ_H and γ_{--} :

$$\cos \gamma_{\text{cen}} = \cos \left(0.4610^{+0.0013}_{-0.0014} \pi \right) - \left(0.020 \, \pm \, 0.002 \right) \ln \varepsilon_{\text{H}} \tag{C19}$$

for $1 \le \varepsilon_{\rm H} < 400$, with a Pearson coefficient of R = 0.80 (p-value < 0.0001; Figure 5, right).

ORCID iDs

Robert Monjo https://orcid.org/0000-0003-3100-2394 Indranil Banik https://orcid.org/0000-0002-4123-7325

References

```
Aalbers, J., Akerib, D. S., Akerlof, C. W., et al. 2023, PhRvL, 131, 041002 Abel, C., Ayres, N. J., Ban, G., et al. 2017, PhRvX, 7, 041034 Angus, G. W., Famaey, B., & Buote, D. A. 2008, MNRAS, 387, 1470 Ardi, E., & Baumgardt, H. 2020, JPCS, 1503, 012023 Asencio, E., Banik, I., Mieske, S., et al. 2022, MNRAS, 515, 2981 Banik, I., & Kalaitzidis, V. 2025, MNRAS, 540, 545 Banik, I., Pittordis, C., Sutherland, W., et al. 2024, MNRAS, 527, 4573 Banik, I., & Zhao, H. 2018, MNRAS, 480, 2660 Banik, I., & Zhao, H. 2022, Symm, 14, 1331 Barkana, R. 2018, Natur, 555, 71 Batygin, K., Morbidelli, A., Brown, M. E., & Nesvorný, D. 2024, ApJL, 966, L8 Bekenstein, J. D. 2004, PhRvD, 70, 083509
```

```
Blanchet, L. 2007, COGra, 24, 3529
Blanchet, L., & Skordis, C. 2024, JCAP, 2024, 040
Brouwer, M. M., Oman, K. A., Valentijn, E. A., et al. 2021, A&A, 650, A113
Brown, K., & Mathur, H. 2023, AJ, 166, 168
Cattaneo, A., Salucci, P., & Papastergis, E. 2014, ApJ, 783, 66
Chae, K.-H. 2022, ApJ, 941, 55
Chae, K.-H. 2023, ApJ, 952, 128
Chae, K.-H. 2024a, ApJ, 960, 114
Chae, K.-H. 2024b, MNRAS, 533, 110
Chae, K.-H., Lelli, F., Desmond, H., et al. 2020, ApJ, 904, 51
Ciufolini, I., Matzner, R., Paolozzi, A., et al. 2019, NatSR, 9, 15881
Comerón, S., Trujillo, I., Cappellari, M., et al. 2023, A&A, 675, A143
Cookson, S. A. 2024, MNRAS, 533, 110
Cyburt, R. H., Fields, B. D., Olive, K. A., & Yeh, T.-H. 2016, RvMP, 88,
de Blok, W. J. G., Walter, F., Brinks, E., et al. 2008, AJ, 136, 2648
De Propris, R., West, M. J., Andrade-Santos, F., et al. 2020, MNRAS,
Desmond, H. 2016, MNRAS, 464, 4160
Desmond, H., Hees, A., & Famaey, B. 2024, MNRAS, 530, 1781
Di Cintio, A., & Lelli, F. 2015, MNRAS Lett, 456, L127
Dittus, H., & Lämmerzahl, C. 2007, AdSpR, 39, 244
Du, P., Egana-Ugrinovic, D., Essig, R., & Sholapurkar, M. 2022, PhRvX, 12,
  011009
Eckert, D., Ettori, S., Pointecouteau, E., van der Burg, R. F. J., & Loubser, S. I.
  2022, A&A, 662, A123
Efstathiou, G., Sutherland, W. J., & Maddox, S. J. 1990, Natur, 348, 705
Faisal ur Rahman, S., & Jawed Iqbal, M. 2019, EPJP, 134, 302
Famaey, B., Khoury, J., Penco, R., & Sharma, A. 2020, JCAP, 2020, 025
Famaey, B., & McGaugh, S. S. 2012, LRR, 15, 10
Goddy, J. S., Stark, D. V., Masters, K. L., et al. 2023, MNRAS, 520, 3895
Grohs, E., & Fuller, G. M. 2022, in Big Bang Nucleosynthesis, ed. I. Tanihata,
  H. Toki, & T. Kajino (Berlin: Springer), 127
Haghi, H., Amiri, V., Hasani Zonoozi, A., et al. 2019, ApJ, 884, L25
Harikumar, S., & Biesiada, M. 2022, EuPhJC, 82, 241
```

```
Haslbauer, M., Banik, I., & Kroupa, P. 2020, MNRAS, 499, 2845
Hees, A., Folkner, W. M., Jacobson, R. A., & Park, R. S. 2014, PhRvD, 89,
   102002
Hernandez, X. 2023, MNRAS, 525, 1401
Hernandez, X., Chae, K.-H., & Aguayo-Ortiz, A. 2024, MNRAS, 533, 729
Hernandez, X., & Kroupa, P. 2025, MNRAS, 537, 2925
Hernandez, X., Verteletskyi, V., Nasser, L., & Aguayo-Ortiz, A. 2023,
    MNRAS, 528, 4720
Hoof, S., Geringer-Sameth, A., & Trotta, R. 2020, JCAP, 2020, 012
Hu, X.-S., Zhu, B.-Y., Liu, T.-C., & Liang, Y.-F. 2024, PhRvD, 109, 063036
Katz, A., Reece, M., & Sajjad, A. 2016, PDU, 12, 24
Keenan, R. C., Barger, A. J., & Cowie, L. L. 2013, ApJ, 775, 62
Kelleher, R., & Lelli, F. 2024, A&A, 688, A78
Kroupa, P. 2015, CJP, 93, 169
Kroupa, P., Gjergo, E., Asencio, E., et al. 2023, PoS, 436, 231
Leauthaud, A., Finoguenov, A., Kneib, J.-P., et al. 2010, ApJ, 709, 97
Lelli, F., McGaugh, S. S., & Schombert, J. M. 2016, ApJ, 152, 157
Lelli, F., McGaugh, S. S., Schombert, J. M., Desmond, H., & Katz, H. 2019,
    INRAS, 484, 3267
Lelli, F., McGaugh, S. S., Schombert, J. M., & Pawlowski, M. S. 2017, ApJ,
   836, 152
Li, P., Tian, Y., Júlio, M. P., et al. 2023, A&A, 677, A24
Liu, X.-H., Li, Z.-H., Qi, J.-Z., & Zhang, X. 2022, ApJ, 927, 28
Mavromatos, N. E., Sakellariadou, M., & Yusaf, M. F. 2009, PhRvD, 79,
  081301
Mazurenko, S., Banik, I., & Kroupa, P. 2025, MNRAS, 536, 3232
Mazurenko, S., Banik, I., Kroupa, P., & Haslbauer, M. 2024, MNRAS,
   527, 4388
McGaugh, S. S. 2004, ApJ, 609, 652
McGaugh, S. S., de Blok, W. J. G., Schombert, J. M., de Naray, R. K., &
   Kim, J. H. 2007, ApJ, 659, 149
McGaugh, S. S., Lelli, F., & Schombert, J. M. 2016, PhRvL, 117, 201101
Melia, F. 2007, MNRAS, 382, 1917
Melia, F. 2017, FrPhy, 12, 129802
Melia, F., & López-Corredoira, M. 2022, IJMPD, 31, 2250065
```

```
Mercado, F. J., Bullock, J. S., Moreno, J., et al. 2024, MNRAS, 530,
  1349
Merritt, D. 2017, SHPMP, 57, 41
Migaszewski, C. 2023, MNRAS, 525, 805
Milgrom, M. 1983, ApJ, 270, 365
Mistele, T., McGaugh, S., Lelli, F., Schombert, J., & Li, P. 2024, ApJL, 969, 3
Mitra, A. 2014, MNRAS, 442, 382
Moffat, J. W. 2006, JCAP, 03, 004
Moffat, J. W., & Toth, V. T. 2009, MNRAS, 397, 1885
Moffat, J. W., & Toth, V. T. 2013, Galax, 1, 65
Monjo, R. 2017, PhRvD, 96, 103505
Monjo, R. 2018, PhRvD, 98, 043508
Monjo, R. 2023, CQGra, 40, 235002
Monjo, R. 2024a, PhD thesis, Complutense Univ. Madrid
Monjo, R. 2024b, ApJ, 967, 66
Monjo, R., & Campoamor-Stursberg, R. 2020, CQGra, 37, 205015
Monjo, R., & Campoamor-Stursberg, R. 2023, CQGra, 40, 195006
Negrelli, C., Benito, M., Landau, S., Iocco, F., & Kraiselburd, L. 2018,
   PhRvD, 98, 104061
Ostriker, J. P., & Steinhardt, P. J. 1995, Natur, 377, 600
Pittordis, C., & Sutherland, W. 2019, MNRAS, 488, 4740
Pittordis, C., & Sutherland, W. 2023, OJAp, 6, 4
Planck Collaboration, Aghanim, N., & Akrami, Y. 2020, A&A, 641, A1
Roshan, M., Ghafourian, N., Kashfi, T., et al. 2021, MNRAS, 508, 926
Seifert, M. D. 2007, PhRvD, 76, 064002
Shi, D., Wang, X., Zheng, X., et al. 2024, ApJ, 963, 21
Skordis, C., & Złośnik, T. 2021, PhRvL, 127, 161302
Stiskalek, R., & Desmond, H. 2023, MNRAS, 525, 6130
Tian, Y., Ko, C.-M., Li, P., McGaugh, S., & Poblete, S. L. 2024, A&A,
  684, A180
Tian, Y., Umetsu, K., Ko, C.-M., Donahue, M., & Chiu, I.-N. 2020, ApJ,
  896, 70
Touboul, P., Métris, G., Rodrigues, M., et al. 2022, CQGra, 39, 204009
Trippe, S. 2014, ZNatA, 69, 173
Vokrouhlický, D., Nesvorný, D., & Tremaine, S. 2024, ApJ, 968, 47
```